Journal of High Energy Physics, Gravitation and Cosmology, 2025, 11(4), 1428-1461
https://www.scirp.org/journal/jhepgc
ISSN Online: 2380-4335
ISSN Print: 2380-4327

The Unification of the Four Fundamental Interactions

Yun Liu[1,2*], Ze Liu[2], Shen Yan[2], Ziyi Liu[2]

[1]Department of Law, Zhengzhou University, Zhengzhou, China
[2]Liu Yun Studio, Tsinghua University, Beijing, China
Email: *lyz-gyl@163.com

How to cite this paper: Liu, Y., Liu, Z., Yan, S. and Liu, Z.Y. (2025) The Unification of the Four Fundamental Interactions. *Journal of High Energy Physics, Gravitation and Cosmology*, **11**, 1428-1461.
https://doi.org/10.4236/jhepgc.2025.114088

Received: June 28, 2025
Accepted: October 8, 2025
Published: October 11, 2025

Abstract

The unification of the four fundamental forces represents the ultimate goal and a major challenge in modern physics, primarily because previous attempts have failed to achieve precise calculations at microscopic scales. In this study, we have derived a universal formula capable of accurately calculating the mass values of particles in each quantum state, achieving unprecedented precision in ultra-microscopic particle computations. Our research findings indicate that both the strong and weak interactions are the result of the collective superposition of internal charge interactions. However, the gravitational effects between masses remain under exploration.

Keywords

Special Relativity, Quantum Mechanics, Particle Physics, Grand Unified Theory, Heavy Quark

1. Introduction

The forces of nature are divided into four categories; however, Einstein believed that these four forces should all originate from the same fundamental essence. Thus, physicists embarked on the path toward the grand unification of the four forces. This endeavor has become an ultimate goal in physics, and many physicists have devoted themselves to this cause. Initially, Glashow and others proposed the electroweak unification theory to unify the weak interaction and the electromagnetic force [1] [2]. Subsequently, through the efforts of Yukawa Hideki, Chen-Ning Yang, and others, the research methods for the strong interaction were also aligned with those of the electromagnetic force. The unification of the four fundamental forces seemed within reach. However, how the strong interactions can

be unified with the electromagnetic force, as well as how gravity can be unified with electromagnetic interactions, remains unclear. In 1974, Samuel C.C. Ting and Burton Richter made the groundbreaking discovery of the J/ψ particle, which immediately attracted significant attention as an ideal probe for studying strong interactions. Shortly thereafter, numerous researchers devoted themselves to this pioneering work [3]-[8]. However, when using the Dirac Equation [9] to calculate the mass of a quarkonium, it resulted in large errors, making it impossible to uncover the underlying rules of the strong interaction.

As early as 2012, Chinese scholar Liu Yun proposed that the strong interaction between particles is a combined relativistic effect of charge forces. However, no one believed this view, so Liu Yun's paper was never approved for publication by any magazine. To find convincing evidence, Liu Yun began organizing our team for dedicated research. First, we developed a universal quantum method capable of accurately calculating the radius of ultra-microscopic particles and the gravitational coefficients between internal particles. Second, we postulated that particles possess spin velocity and derived a formula for the gravitational coefficient between any particles based on special relativity. This formula depends solely on distance and spin rate. Finally, we compared the variation patterns of the gravitational coefficient between quarks with distance and found that the formula for the interquark gravitational coefficient perfectly matches our derived formula. Further research revealed that both gravitational mass and weak interactions conform to the gravitational coefficient formula, proving that all forces can be unified as the electromagnetic force. Our approach maintains rigorous mathematical derivation while achieving full consistency with experimental data, thereby establishing a new paradigm for studying ultra-microscopic phenomena.

2. Materials and Methods

2.1. How to Calculate the Radius of a Two-Body Particle

Here, we take the hydrogen atom as an example to derive the particle radius. In quantum mechanics, approximation methods are frequently employed to solve problems. Based on the degenerate mass of particles, we construct the following approximate equation:

$$m_e\sqrt{1-\frac{a^2}{n^2}} \approx m-V, m=\frac{m_e}{\sqrt{1-v^2}}, V=\frac{am_e v}{L\sqrt{1-v^2}}, L=\sqrt{l\left(l+1\right)}, c=\hbar=1 \quad (1)$$

Derive the expression for the orbital velocity of the electron from Equation (1):

$$v \approx \frac{a}{L}\left(1\pm\sqrt{1-\frac{L^2}{n^2}}\right), L \approx n \quad (2)$$

This corresponds to the velocities at the two extremal points of an elliptical orbit. Assuming the closest point is point-A, and the farthest point is point-B. Therefore, the average radius of the orbit should be:

$$\left.\begin{array}{l}\langle r_1\rangle=\dfrac{r_A+r_B}{2}=\dfrac{L}{2(1+b)}\left(\dfrac{\hbar}{m_1v_A}+\dfrac{\hbar}{m_1v_B}\right),L\approx\sqrt{l(l+1)}\\ v_A\approx\dfrac{a}{L}\left(1-\sqrt{1-\dfrac{L^2}{n^2}}\right),v_B\approx\dfrac{a}{L}\left(1+\sqrt{1-\dfrac{L^2}{n^2}}\right)\end{array}\right\}\langle r_1\rangle=\frac{n^2\hbar\sqrt{1-v_1^2}}{m_{10}a} \quad (3)$$

Here, r_A is the distance from point A to the focus, and r_B is the distance from point B to the focus. However, since we need to generalize the equation to two-body particle systems while maintaining applicability to high-speed spinning particles, we have made the following modifications:

$$\left.\begin{array}{l}m_1v_1r_1+m_2v_2r_2=(1+b)m_1v_1r_1=L\hbar,b=\dfrac{m_1}{m_2}\\ m_1=\dfrac{m_{10}}{\sqrt{1-v_1^2}},v_1=\dfrac{a}{(1+b)n},L=\sqrt{l(l+1)}\neq0\end{array}\right\}\rightarrow r_1=\frac{nL\hbar\sqrt{1-v_1^2}}{m_{10}a} \quad (4)$$

Here, m_{10} is the rest mass of a particle 1, and m_1 is the relativistic mass of the lighter particle, a is the coefficient of attraction between two particles, and r_1 is the orbital radius of particle 1. On the other hand, according to quantum mechanics, the following averaging equation is introduced:

$$\left.\begin{array}{l}\left\langle\dfrac{1}{r_1^2}\right\rangle=\dfrac{1}{n^3(l+1/2)r_0^2}\\ d_0=(1+b)r_0,b=\dfrac{m_1}{m_2},c=1\end{array}\right\}\rightarrow r_1\approx nr_0\sqrt{n\left(l+\frac{1}{2}\right)}\approx n\left(l+\frac{1}{2}\right)\frac{\hbar\sqrt{1-v_1^2}}{m_{10}a} \quad (5)$$

Here, the symbol $<1/r^2>$ represents the average value of $1/r^2$. Generally, when we refer to the spin radius and spin rate of a particle system, we are discussing the average orbital radius and orbital velocity of the lighter particle. Therefore, m_1 represents the mass of the lighter particle, while m_2 denotes the mass of the heavier particle. The mass ratio b cannot exceed 1. In conclusion, our improvement mainly lies in adding the relativistic factor to the Equation, which can explain why the radius of electrons is so small.

2.2. The Gravitational Coefficient between Hydrogen and Electrons

According to **Figure 1**, the interaction force between moving charges at low velocities is given by:

$$\begin{array}{l}F=\dfrac{q_1q_2a_e}{d^2\sqrt{1-v_{1\pm2}^2}}\approx\dfrac{q_1q_2a_e}{d^2}\left(1+\dfrac{v^2}{2}\right)\approx q_2E_1+q_2v\times B_1,a_e\approx\dfrac{1}{137},\\ c=1,v\approx v_{1\pm2}=\dfrac{v_1\pm v_2}{1\pm v_1v_2},E_1=\dfrac{q_1a_e}{d^2},B_1=\dfrac{q_1va_e}{2d^2}=\dfrac{I_1a_e}{2d^2},I_1=q_1v\end{array} \quad (6)$$

At high velocities, due to the periodic positional alternation of two charges in circular motion—where additive and subtractive superposition occur once per revolution—the expression for the average magnetic force between them is:

$$\langle F_B\rangle=q_2v\times B_1=\frac{q_1q_2a_e}{d^2}(\beta_{1\pm2}-1),\beta_{1\pm2}=\frac{1}{\sqrt{1-v_{1\pm2}}} \quad (7)$$

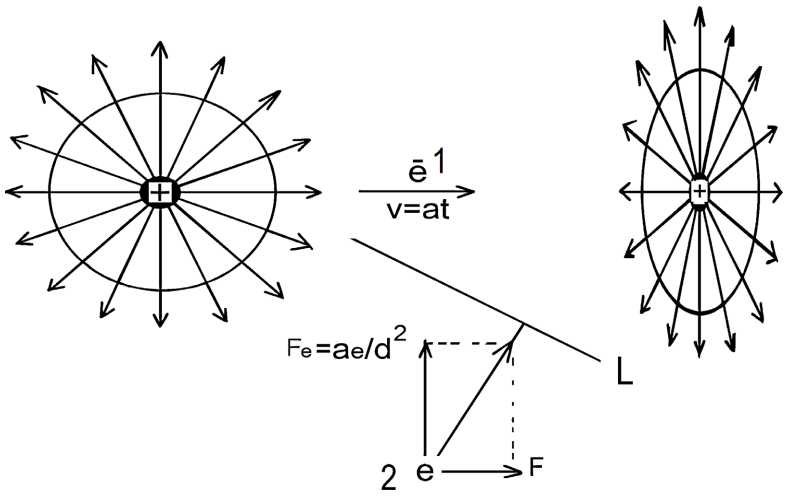

Figure 1. The essence of magnetic fields is a relativistic effect. Relative motion causes the electric field of a moving charge to strengthen in the perpendicular direction while weakening in the longitudinal direction. The accelerated motion of charge 1 distorts its electric field equipotential lines (L), making them non-parallel to its direction of motion, thereby inducing an electric force (F) on charge 2. This is precisely why accelerated charges generate induced electromotive force.

We often encounter situations where particles have different radii, such as protons and electrons forming hydrogen atoms. If the electron's radius is very small, its spin rate will be very high. First, assuming the electron and proton spin antiparallel (with $S = 0$). Since the electron's spin period is much shorter than the proton's, when the proton's valence charge is closest to the electron, the electron's valence charge is also precisely closest to the proton, as shown in **Figure 2(A)**. Meanwhile, the situation in **Figure 2(B)** may also occur. When the configuration is as shown in **Figure 2(A)**, we first neglect the influence of other charges and only consider the magnitude of electrostatic attraction between the two closest charges, giving the following formula:

$$F_{1e} \approx \frac{a_e}{d^2}\frac{1}{\left(1-\Sigma\right)^2}, a_e \approx \frac{1}{137}, \Sigma = \frac{r_p + r_e}{d}, \Delta = \frac{r_p - r_e}{d} \tag{8}$$

When considering only magnetic forces (excluding electrostatic forces), the resultant magnetic force exerted by charge 3 on charges 4, 5 and 6 is given by (see **Figure 2(A)**):

$$\begin{gathered}\left\langle F_{3B}\right\rangle_{3^*(4+5+6)} = a_e\left[-\frac{q_3q_4\left(\beta_{e+p-4}-1\right)}{\left(d-2r-r_4\right)^2}+\frac{q_3q_5\left(\beta_{e+p+5}-1\right)}{\left(d-2r+r_5\right)^2}-\frac{q_3q_6\left(\beta_{e-p}-1\right)}{d^2}\right], \\ \beta_{e+p-4} = \frac{1}{\sqrt{1-v_{e+p-4}}}, v_{e+p-4} = \frac{v_{e+p}-v_4}{1-v_{e+p}v_4}, v_{e+p+5} = \frac{v_{e+p}+v_5}{1+v_{e+p}v_5}, v_{e+p} = \frac{v_e+v_p}{1+v_ev_p}\end{gathered} \tag{9}$$

Here, positive charges denoted by "+", negative charges by "−"; and "+" in results indicates repulsion, "−" indicates attraction. Due to the differing spin periods of protons and electrons, Charge 3 in **Figure 2(A)** may exhibit either subtractive superposition (50% probability) or additive superposition (50% probability) with

Charge 6.

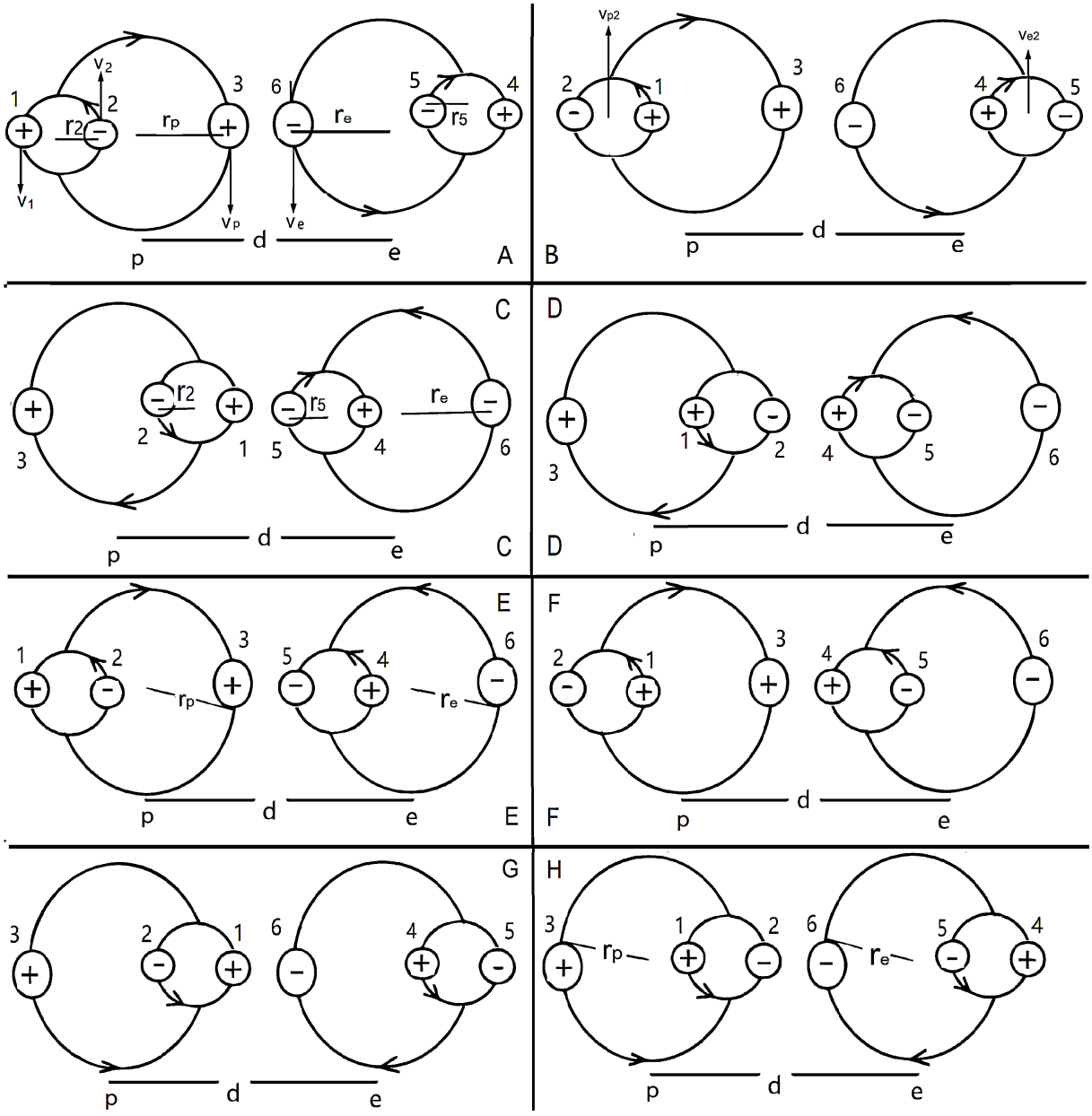

Figure 2. Possible charge distribution patterns during proton-electron coupling at $S = 0$.

When distance effects are neglected, the average magnetic interaction force between Charge 3 and Charge 6 is given by:

$$\begin{aligned}&\langle F_{3^*6}\rangle_{e-p} = -\frac{q_3 q_6 a_e}{d^2}\left[1+\left(\beta_{e-p}-1\right)\right], \langle F_{3^*6}\rangle_{e+p} = -\frac{q_3 q_6 a_e}{d^2}\left[1+\left(\beta_{e+p}-1\right)\right],\\ &\langle F_{3^*6}\rangle = \frac{\langle F_{3^*6}\rangle_{e-p}+\langle F_{3^*6}\rangle_{e+p}}{2} = -\frac{q_3 q_6 a_e}{d^2}\left[1+\left(\beta_e\beta_p-1\right)\right], \frac{\beta_{e-p}+\beta_{e+p}}{2} = \beta_e\beta_p\end{aligned} \tag{10}$$

Thus, at long distances (when proton radius effects are negligible), the total combined interaction force between protons and electrons is given by:

$$\left.\begin{array}{l}\left(\beta_p-\beta_2\beta_{p2}+\beta_1\beta_{p2}-1\right)\approx\dfrac{\mu_p}{d}\\ \left(-\beta_e+\beta_4\beta_{e2}-\beta_5\beta_{e2}+1\right)\approx\dfrac{\mu_e}{d}\end{array}\right\}\left\langle F_{ep}\right\rangle\approx-\frac{a_e}{d^2}\left(q_eq_p+\frac{\mu_p\mu_e}{d^2}\right)\tag{11}$$

Equation (11) shows that when particles are far apart, their magnetic interaction approaches zero. This explains why electrons exhibit purely charge-based forces at long distances, while allowing for annihilation effects at close range.

As analyzed in Figure 2, particles with negligible radii exhibit near-complete cancellation of gravitational influence regardless of spin orientation variations. The dominant contribution to gravitational modulation stems exclusively from unpaired charges—termed valence charges of protons or electrons. From relativistic principles, we derive the following governing rule:

$$\begin{array}{l}\beta_{e\pm p}=\left(1\pm v_ev_p\right)\beta_e\beta_p,\left(\beta_{e+p}-\beta_{e-p}\right)=2v_ev_p\beta_e\beta_p,\\ \left(\beta_{e+p}+\beta_{e-p}\right)=2\beta_e\beta_p,\beta_{e-p}=\beta_{e+p}\dfrac{1-v_ev_p}{1+v_ev_p}\end{array}\tag{12}$$

When evaluating exclusively the valence-originating magnetogravitic coupling through ensemble averaging over Figure 2 (Only calculate $\boldsymbol{F}_{3*6}$). Figure 2(A)-(H)'s topological configurations, the $S=0$ proton-electron system exhibits a mean magnetic attraction of:

$$\begin{array}{l}\left\langle F_B\right\rangle_{ep,s=0}=\dfrac{1}{8}\left\langle F_B\right\rangle\left(A+B+C+D+E+F+G+H\right)\\ \approx-\dfrac{a_e}{2d^2}\left[\dfrac{1+\Sigma^2}{\left(1-\Sigma^2\right)^2}\left(\beta_{e-p}-1\right)+\dfrac{1+\Delta^2}{\left(1-\Delta^2\right)^2}\left(\beta_{e+p}-1\right)\right]-F_{0B}\\ \approx-\dfrac{a_e}{d^2}\left[\dfrac{1+\Sigma^2-2r_pr_e\left(1+v_ev_p\right)/d^2}{\left(1-\Sigma^2\right)^2}\beta_p\beta_e-1\right]-F_{0B},\\ \beta_{e-p}\gg1,\beta_{e+p}\gg1,d\gg r_p+r_e,F_{0B}=F_{B3*(4+5)}+F_{B(4+5+6)*(1+2)}\end{array}\tag{13}$$

In the formula, $F_{B3*(4+5)}$ represents the resultant magnetic force between charge 3 and charges (4,5). Since gravitational and repulsive forces nearly cancel out, the magnitude F_{0B} is significantly smaller than the valence charge magnetic force and can generally be neglected in strong interaction calculations.

Applying the same computational method, the average magnetic attraction between protons and electrons at $S=1$ is given by:

$$\begin{array}{l}\left\langle F_B\right\rangle_{ep,s=1}\approx-\dfrac{a_e}{2d^2}\left[\dfrac{1+\Sigma^2}{\left(1-\Sigma^2\right)^2}\left(\beta_{e+p}-1\right)+\dfrac{1+\Delta^2}{\left(1-\Delta^2\right)^2}\left(\beta_{e-p}-1\right)\right]-F_{0B}\\ \approx-\dfrac{a_e}{d^2}\left[\dfrac{1+\Sigma^2-2r_er_p\left(1-v_ev_p\right)/d^2}{\left(1-\Sigma^2\right)^2}\beta_e\beta_p-1\right]-F_{0B}\end{array}\tag{14}$$

The hyperfine splitting energy ($\Delta E=5.87$ μeV) between the ground-state hydrogen's singlet ($S=0$) and triplet ($S=1$) configurations—arising from electron-

proton spin-spin magnetic coupling—manifests observationally as the 1420.4 MHz (21 cm) spectral line:

$$\Delta V = d\left(\left\langle F_B\right\rangle_{S=0} - \left\langle F_B\right\rangle_{S=1}\right) \approx \frac{4a_e}{d}\frac{r_e r_p v_e v_p \beta_e \beta_p}{d^2} \tag{15}$$

Evidently, this energy difference is proportional to the product of the electron and proton spin magnetic moments. A more precise calculation requires quantum mechanical (see Section 2.5). Here, we only estimate the order of magnitude. In the equation, $d = a_0 \approx 0.53 \times 10^{-11}$ m (Bohr radius), $a_e/d = 27.2$ eV, $v_e \approx 1$. The magnetic potential energy difference $\Delta V \approx 5.87 \times 10^{-6}$ eV. Proton radius: 0.83 fm; Proton spin rate: 0.93c (see Section 2.9). Thus:

$$\left.\begin{aligned} v_e r_e \beta_e &\approx 7\times 10^{-14}\ \text{m} \\ v_e \beta_e &= \frac{1}{\sqrt{1/v_e^2 - 1}} \end{aligned}\right\} \rightarrow \begin{cases} r_e = 10^{-19}\ \text{m}, v_e \approx 0.999\cdots(12\ \text{nines}) \\ r_e = 10^{-20}\ \text{m}, v_e \approx 0.999\cdots(14\ \text{nines}) \\ r_e = 10^{-21}\ \text{m}, v_e \approx 0.999\cdots(16\ \text{nines}) \end{cases} \tag{16}$$

The above calculations indicate that the radius of an electron is very small and its spin rate is very high. In Section 2.7, we will present an alternative method for calculating the electron's radius and magnetic moment. Finally, we give that the gravitational coupling coefficient between particles of opposite charge is expressed as:

$$\begin{aligned} \left\langle a\right\rangle_{s=1} &\approx a_e + \frac{a_e}{2}\left[\frac{1+\Sigma^2}{\left(1-\Sigma^2\right)^2}\left(\beta_{1+2}-1\right) + \frac{1+\Delta^2}{\left(1-\Delta^2\right)^2}\left(\beta_{1-2}-1\right)\right] - d^2 F_{0B} \\ \left\langle a\right\rangle_{s=0} &\approx a_e + \frac{a_e}{2}\left[\frac{1+\Sigma^2}{\left(1-\Sigma^2\right)^2}\left(\beta_{1-2}-1\right) + \frac{1+\Delta^2}{\left(1-\Delta^2\right)^2}\left(\beta_{1+2}-1\right)\right] - d^2 F_{0B} \end{aligned} \tag{17}$$

When two particles possess identical spin radii and rotation rates while carrying opposite charges, they form mutually reciprocal particles. Examples include positronium, protonium, or quarkonium systems. The gravitational coupling coefficient between their constituent particles is given by:

$$\begin{aligned} \left\langle a_{p\bar{p}}\right\rangle_{s=1} &\approx a_e + \frac{a_e}{2}\frac{1+4r^2/d^2}{\left(1-4r^2/d^2\right)^2}\left(\beta_{2p}-1\right) - d^2 F_{0B} \\ \left\langle a_{p\bar{p}}\right\rangle_{s=0} &\approx a_e + \frac{a_e}{2}\left(\beta_{2p}-1\right) - d^2 F_{0B}, \beta_{2p} = \frac{2v_p}{1+v_p^2} \end{aligned} \tag{18}$$

This explains why the energy state is always lower when positive and negative magnetic moments have parallel spins (this is also known as pairing energy).

2.3. How to Accurately Calculate the Mass of Each Quantum State of a Particle

Previously, we did not understand which factors were related to particle mass, leading to a series of difficulties. In 2015, our team revisited the statistical laws governing particle mass and discovered that the mass of a particle is strictly equal to the sum of the total energy and total potential energy of its internal orbiting

particles. Based on this discovery, we derived the relativistic form of the Hamiltonian and expressed the eigenvalue equation of the particle as [10]:

$$\left.\begin{array}{l} M = m + V \to \left(m + V - M\right)\psi_{x,y,z,t} = 0 \\ H = M - m_0 = m + V - m_0, E\psi = H\psi \end{array}\right\} i\hbar\frac{\partial}{\partial t}\psi = \left(m + V - m_0\right)\psi \tag{19}$$

Here, M represents the rest mass of the particle system, H stands for Hamiltonian, m is the sum of the energies of all orbital particles within the particle, this refers to the relativistic mass. V is the sum of the potential energies between all orbital particles, with attractive potential energies counted as negative values and repulsive potential energies counted as positive values. When the spin rate of a particle is very low, Eq. 19 becomes the Schrodinger equation:

$$\left.\begin{array}{l} m = \dfrac{m_0}{\sqrt{1-v^2}} \xrightarrow{v\to 0} m_0\left(1+\dfrac{v^2}{2}\right), \dfrac{m_0 v^2}{2} \approx \dfrac{p^2}{2m} \\ H = m + V - m_0 = \dfrac{m_0 v^2}{2} + V, E\psi = H\psi \end{array}\right\} \to i\hbar\frac{\partial}{\partial t}\psi = \left(\frac{p^2}{2m} + V\right)\psi \tag{20}$$

Referring to the work achievements of Sommerfield and Dirac, we present the following equation [11].

$$\begin{aligned} M = & \frac{m_{10}}{\sqrt{1+\dfrac{a^2/(1+b)^2(l+1)^2}{\left[\dfrac{n}{l+1}-1+\sqrt{1-\dfrac{a^2}{(1+b)^2(l+1)^2}}\right]^2}}} \\ & + \frac{m_{20}}{\sqrt{1+\dfrac{a^2b^2/(1+b)^2(l+1)^2}{\left[\dfrac{n}{l+1}-1+\sqrt{1-\dfrac{a^2b^2}{(1+b)^2(l+1)^2}}\right]^2}}} \end{aligned} \tag{21}$$

Here, n is the principal quantum number, l is the orbital angular momentum quantum number, M is the rest mass of the quark particle, and a is the gravitational coefficient of the n-th principal shell, $b = m_1/m_2$ is the dynamic mass ratio of the orbital particles. Regardless of the nature of the gravitational force that forms bound-state particles, the quantum rules they follow are consistent. Therefore, this equation is applicable to all two-body particles, including binary star systems. Essentially, each particle behaves as a microscopic magnet. The distinct coupling configurations and resultant spin combinations manifest as orientation variations between these magnetic dipoles, reflecting differential charge motion trajectories. According to relativistic principles, such variations induce modifications in the gravitational coupling coefficients. While the equation form remains invariant, the coefficients exhibit subtle quantum-state-dependent variations—this fundamentally accounts for hydrogen's hyperfine structure. Crucially, incorporating this conceptual advancement into Equation (21) renders them universally applicable across all quantum states of all particles.

In 2023, Liu Zhe proposed an energy splitting equation for quarkonium triplet states to enable precise calculation of the mass of each quantum state in quarkonium systems:

$$\left.\begin{aligned}\Delta V_{LS} &= \frac{a_{nl}\mu_1\mu_2\sigma}{2m_1^2}\frac{l(l+1)}{f(f+1)}\langle LS\rangle\left\langle\frac{1}{d^3}\right\rangle \\ \left\langle\frac{1}{d^3}\right\rangle &= \frac{m_0^3 a_{nl}^3}{(1+b)^3 n^3\hbar^3}\frac{1}{l(l+1)(l+1/2)} \\ A &= \frac{m_0 a_{nl}^4\mu_1\mu_2\sigma\beta_{nl}}{(1+b)^3 n^3 l(l+1)(2l+1)\sqrt{1-v_{nl}^2}}\end{aligned}\right\}\Delta V_{LS} = \begin{cases}+Al^2/(l+2), & f = l+S \\ -A, & f = l+0 \\ -A(l+1)^2/(l-1), & f = l-S\end{cases} \quad (22)$$

Here σ is the error coefficient, μ_1 is the spin magnetic moment of particle 1; μ_2 is the spin magnetic moment of particle 2. Theoretically, the error coefficient is related to the coupling method of the particle's spin magnetic moment. When calculating the interaction coefficient, we have already taken the spin coupling method into account. Even if there are errors, they can be adjusted by selecting different gravitational coefficients. Therefore, we let $\sigma\mu_1\mu_2 = 1$. The computational results of this equation demonstrate remarkable accuracy, substantially exceeding our previous studies, though minor discrepancies persist for low-n states. A year later, Liu Ziyi proposed a groundbreaking insight: the results computed from Equation (22) only modified the potential energy, which is not entirely equivalent to mass. This was a remarkably bold proposition—though it contradicted established textbook theories, the calculated results showed excellent agreement with experimental data, especially with improved accuracy for low-n states. According to Liu Ziyi's method, the gravitational coefficient for each quantum state should be calculated using the following equation:

$$\left.\begin{aligned}\frac{1}{\beta_{nl}} &= \sqrt{1-\frac{a_{nl}^2}{(1+b)^2 n^2}}, \left\langle\frac{1}{d_{nl}}\right\rangle = \frac{m_1 a_{nl}}{n^2\hbar(1+b)} \\ \frac{1}{\beta_{nlf}} &= \sqrt{1-\frac{a_{nlf}^2}{(1+b)^2 n^2}}, \left\langle\frac{1}{d_{nlf}}\right\rangle = \frac{m_1 a_{nlf}}{n^2\hbar(1+b)}\end{aligned}\right\}\begin{cases}\Delta V_{LS} = \dfrac{a_{nl}}{d_{nl}} - \dfrac{a_{nlf}}{d_{nlf}} \rightarrow \\ a_{nlf}^2 = \left(1-\dfrac{n^2\Delta V_{LS}}{m_{nl}a_{al}^2}\right)\dfrac{a_{nl}^2\beta_{nl}}{\beta_{nlf}}\end{cases} \quad (23)$$

In the equation a_{nlf} represents the gravitational coefficient for the n-th principal layer, the l-th sub-layer, and the total spin f. By solving Equation (23), we obtain the analytical expression for the square of a_{nlf}:

$$a_{nlf}^2 = \frac{K^2}{2(1+b)^2 n^2}\left(\sqrt{\frac{4(1+b)^4 n^4}{K^2}+1}-1\right)\begin{cases}K = \left[1-n^2\dfrac{(1+b)\Delta V_{LS}}{m_{nl}a_{al}^2}\right]a_{nl}^2\beta_{nl} \\ \dfrac{1}{\beta_{nl}} = \sqrt{1-\dfrac{a_{nl}^2}{(1+b)^2 n^2}}\end{cases} \quad (24)$$

To obtain the mass in the f-state, the gravitational coefficient derived from the above equation must be substituted into Equation (21). For quarkonium states, when $b = 1$, the following relation holds:

$$\left.\begin{aligned} M &= \frac{2m_{10}}{\sqrt{1+\dfrac{a^2/4(l+1)^2}{\left[\dfrac{n}{l+1}-1+\sqrt{1-\dfrac{a^2}{4(l+1)^2}}\right]^2}}} \\ a_{nlf}^2 &= \frac{K^2}{8n^2}\left(\sqrt{\frac{64n^4}{K^2}+1}-1\right) \end{aligned}\right\} K = \begin{cases} \left[1-\dfrac{la_{nl}^2}{4n(l+1)(l+2)(2l+1)}\right]a_{nl}^2\beta_{nl}, & f=l+S \\ \left[1+\dfrac{a_{nl}^2}{4nl(l+1)(2l+1)}\right]a_{nl}^2\beta_{nl}, & f=l+0 \\ \left[1+\dfrac{(l+1)a_{nl}^2}{4nl(l-1)(2l+1)}\right]a_{nl}^2\beta_{nl}, & f=l-S \end{cases} \quad (25)$$

According to Equation (25), we can calculate the mass of each quantum state in quarkonium systems. For example, substituting $a = 7.31$, $n = 5$, and $l = 4$ into Equation (25), we immediately obtain three distinct gravitational coefficients. These are then substituted and $m_{10} = 2282$ into Equation (25) to derive the triplet mass of the quantum state with $n = 5$ and $l = 4$:

$$a_{nlf} = \frac{K^2}{8n^2}\left(\sqrt{1+\frac{64n^4}{K^2}}-1\right) \rightarrow \begin{cases} a_{545} \approx 7.215874, M_{545} \approx 3159.72, & f = l+S = 5 \\ a_{544} \approx 7.344173, M_{544} \approx 3097.58, & f = l+0 = 4 \\ a_{543} \approx 7.577588, M_{543} \approx 2978.17, & f = l\text{-}S = 3 \end{cases} \quad (26)$$

The calculation results show that the mass states 3097 and 2980 surprisingly belong to the same triplet group. Before this, there was significant controversy regarding the classification hierarchy of the 2980 quantum states. Our calculations reveal that accompanying the 3097 state is a 3160 mass datum—representing a previously undiscovered quantum state. We maintain that this provides an ideal opportunity for experimental verification of our theoretical computations' accuracy. Using the same method, substitute $a = 7.291$, $n = 6$, $l = 4$ and $m_{10} = 2282$ into Equation (25):

$$a_{nlf} = \frac{K^2}{8n^2}\left(\sqrt{1+\frac{64n^4}{K^2}}-1\right) \rightarrow \begin{cases} a_{645} \approx 7.196991, M_{645} \approx 3555.6, & f = l+S = 5 \\ a_{644} \approx 7.325426, M_{644} \approx 3508.9, & f = l+0 = 4 \\ a_{643} \approx 7.567511, M_{643} \approx 3415.3, & f = l-S = 3 \end{cases} \quad (27)$$

To ascertain the precise mass of the quark c, we conducted extensive calculations and comparisons. This comparative verification work, spanning over a decade, involved extensive computational efforts. **Table 1** below presents one representative example from our numerous comparative studies [11].

Table 1. Comparison of simulation results for quarks with different masses.

	$m_0 = 2270$	$m_0 = 2282$	Experimental data
$a_{5,4}$	$a_{5,4} = 7.222$	$a_{5,4} = 7.31$	-
$^3M_{5,4}$	2981.6-3097.1-3158.3	2978.2-3097.6-3159.7	2979.7-3096.9-no
$a_{6,4}$	$a_{64} = 7.147$	$a_{64} = 7.291$	-
$^3M_{6,4}$	3420.6-3511.7-3554.7	3415.3-3508.8-3555.6	3415.1-3510.5-3556.2
$a_{7,6}$	$a_{76} = 6.276$	$a_{76} = 6.611$	-
$^3M_{7,6}$	4010.2-4023.6-4028.7	4009.0-4021.6-4029.6	4009-4021.5-4030

The calculations indicate that only when the mass of the quark c is 2282 can it align with the experimental values. Consequently, the mass number, spin number, and charge number of the quark c are identical to those of the ordinary Λc particle. This discovery reveals that certain high-spin particles exhibit strong interactions at close range while behaving like ordinary particles at larger distances. Precisely because these ordinary particles carry a unit charge ($q = 1$), and our equations are calculated based on this unit charge, the results achieve unprecedented agreement with experimental data. We therefore conclude that quarks are such ordinary particles whose charges must be integer-valued rather than fractional. Research on other quarkonium states corroborates this finding, for instance, studies on the ϒ particle suggest that the mass of the bottom quark is 5580, with spin and mass numbers very close to those of the ordinary Λ_b particle. Therefore, when Λ_b transforms into the bottom quark, its mass changes from 5500 to 5580, and its charge number increases by 1, analogous to the change in mass when a neutron transforms into a proton.

According to Equation (25), we get the following **Table 2** [11].

Table 2. The calculated masses of the J/ψ particle triplet states.

	$n = 5$	$n = 6$	$n = 7$	$n = 8$
$l = n - 1$	$a \approx 7.31$ 2978-3097-3160	$a \approx 6.749$ 3737-3769-3794	$a \approx 6.611$; 4009-4022-4030	$a \approx 6.572$; 4153-4160-4162
$l = n - 2$	0	$a \approx 7.291$; 3415-3509-3556	$a \approx 7.288$; 3823-3854-3872	$a \approx 7.312$ 4025-4040-4049
$l = n - 3$	0	0	$a \approx 7.621$ 3594-3679-3723	$a \approx 7.747$ 3900-3930-3946
$l = n - 4$	0	0	0	$a \approx 8.057$ 3686-3770-3811

The number 0 in the table indicates that this quantum state does not exist.

In **Table 2**, a is the corresponding gravitational coefficient. The underlined data in the table represent the mass numbers that have been experimentally discovered. According to the calculations, the experimental value 3885 corresponds to the triplet state with $n = 9$ and $l = 4$, therefore, it is not listed in **Table 2**.

In previous studies of the J/ψ particle, we always considered the ground state to be $n = 1$, not only were the margins of error considerable, but there was also a plethora of experimental data that defied explanation, which the physics community termed as exotic energy levels [12] [13]. The research outcomes of our team have adeptly resolved these conundrums, with all experimental data aligning impeccably with the calculated values. It is evident that the so-called anomalous energy levels previously discussed in the physics community were merely a result of the lack of correct computational methods.

2.4. How to Determine Suspended State Particles

In our calculations, we discovered that some particles lack the $n = 1$ quantum state. Such particle systems have been named "Suspended State Particles" by Liu Yun. This is a significant discovery as it provides an explanation for why many particles (such as the electron) exhibit only a single quantum state. How do we determine whether a quantum state exists for a particle? First, we assume the spin rate and radius of the quark and aim to obtain data consistent with experimental values. The calculations indicate that the spin rate of quark c is about 0.999436c and a spin radius of 3.66×10^{-17} m = 0.0366 fm. Under these conditions, according to Equation (18), we omit the less significant terms in the formula and obtain the equation for the gravitational coefficient between quark c and anti-quark c (with $S = 1$):

$$\begin{aligned}\left\langle a_{c\bar{c}}\right\rangle_{S=1} &\approx a_e + \frac{a_e}{2}\frac{1+\left(2r/d\right)^2}{\left[1-\left(2r/d\right)^2\right]^2}\left(\beta_{c+c}-1\right)-d^2F_{0B} \\ &\approx \frac{a_e}{2}\frac{1+\left(2r/d\right)^2}{\left[1-\left(2r/d\right)^2\right]^2}\beta_{c+c} \approx 6.465\frac{1+\left(2r/d\right)^2}{\left[1-\left(2r/d\right)^2\right]^2}, \beta_{c+c}=\frac{1}{\sqrt{1-v_{c+c}^2}}\end{aligned} \tag{28}$$

Using the same computational method, we determine that the radius of the bottom quark (quark b) is approximately 4.1×10^{-17} m (0.041 fm), with a spin rate of about $0.999437c$. Only these precise values yield results consistent with experimental data. Consequently, based on Equation (18), the gravitational coefficient equation between a quark b and its antiparticle (anti-quark b) is:

$$\left\langle a_{b\bar{b}}\right\rangle_{S=1} \approx \frac{a_e}{2}\frac{1+4r^2/d^2}{\left(1-4r^2/d^2\right)^2}\beta_{b+b} \approx 6.4815\frac{1+4r^2/d^2}{\left(1-4r^2/d^2\right)^2}, d=\left(1+b\right)r_1 \tag{29}$$

Table 3 is the result of our calculation of the gravitational coefficient between quarks using the above Equation (25) and Equation (29) [11].

Table 3. The calculated masses of the ϒ particle triplet states.

	$n = 6$	$n = 7$	$n = 8$	$n = 9$	$n = 10$
$l = n - 1$	0	$a \approx 7.478$ 9379-9429-9460	$a \approx 6.975$ 10023-10042-10054	$a \approx 6.71$; 10347-10355-10361	$a \approx 6.42$; 10566-10570-10573
$l = n - 2$	0	0	$a \approx 7.278$; 9860-9892-9913	$a \approx 7.055$; 10232-10246-10256	$a \approx 6.95$ 10446-10453-10458
$l = n - 3$	0	0	0	$a \approx 7.481$ 10060-1087-11103	$a \approx 7.35$ 10335-10348-10356
$l = n - 4$	0	0	0	0	$a \approx 7.608$ 10233-10255-10269

The underlined numbers are the mass states that have been discovered.

With the gravitational coefficient Equation (29), we can determine which energy levels of the ϒ particle can exist stably. This method is called the Approximation Correction Method, which we developed from the work of the American physicist Feynman. This rule applies to all particles, including hydrogen atoms.

First, having confirmed the genuine existence of the $n = 7$ quantum state, we substitute $m_0 = 5580$ and $a = 7.478$ into Equation (5), calculating the radius of the ϒ-particle at principal quantum number $n = 7$ to be approximately 0.188 fm. Using Equation (21), we determine the mass of this state to be about 9460.

Second, we estimate the radius for the $n = 6$ principal quantum level based on quantum mechanical principles. The radius r_6 of the $n = 6$ level is extrapolated from the $n = 7$ radius r_7 through the relation: $r_6 = (36/49)r_7 \approx 0.145$ fm.

Third, we perform radius correction for the $n = 6$ state: Input the estimated radius into Equation (29) to obtain the strong interaction coefficient $a = 8$ for the $n = 6$ quantum state. Substitute $a = 8$ back into Equation (5) to derive a corrected radius value.

Fourth, we adjust the gravitational coefficient for the $n = 6$ quantum state by: Inserting the revised radius into Equation (29). Computing an updated gravitational coefficient.

Fifth, we implement an iterative correction procedure. Through multiple cycles of mutual refinement: If errors progressively amplify → This indicates the ϒ-particle cannot maintain stable configuration at $n = 6$ level, confirming its non-existence. If errors consistently diminish and converge to zero → This verifies a stable, physically realizable quantum state.

Our computational results demonstrate that the ϒ-particle cannot stably exist in the $n = 6$ quantum state, confirming the non-existence of this state.

2.5. How to Calculate the Hyperfine Energy Levels of Hydrogen Atoms

For decades, extraordinarily precise measurements of cosmic 21 cm hydrogen line frequencies have been achieved, reaching remarkable levels of accuracy. However, despite exhaustive computational efforts through various methodologies, persistent minor discrepancies between theoretical predictions and experimental values have remained unexplained. In different particle systems, the form of spin coupling varies due to differences in particles' spin magnetic moments and masses. However, spin does not alter the fundamental quantum rules—it only modifies the magnitude of interaction coefficients. Based on this theory, we incorporate all particle systems into the quantum mechanical framework governed by Equation (21), including the hyperfine structure splitting rules of hydrogen atoms.

When $n = 1$, $l = 0$, $j = 1/2$, $s_2 = 1/2$, it corresponds to the ground state of the hydrogen atom. Proton-electron spin coupling—with quantum mechanics prescribing the resultant hyperfine splitting as:

$$\left.\begin{aligned} V_{JS} &= -\frac{a_{nl} g_p g_e}{2m_1^2} \frac{l(l+1)}{j_1(j_1+1)} \left\langle \frac{1}{d^3} \right\rangle \langle IJ \rangle \\ \langle IJ \rangle &= \frac{1}{2}\left(F^2 - J^2 - I^2\right), \hbar = 1 \\ \left\langle \frac{1}{d^3} \right\rangle &= \left[\frac{m_1 a_{nl}}{(1+b)n}\right]^3 \frac{1}{l(l+1)(l+1/2)} \end{aligned}\right\} \rightarrow V_{JS} = \begin{cases} -\dfrac{m_1 a_{nl}^4 g_e g_p}{3(1+b)^3 n^3}, f = j_1 + s_2 = 1 \\ +\dfrac{m_1 a_{nl}^4 g_e g_p}{(1+b)^3 n^3}, f = j_1 - s_2 = 0 \end{cases} \tag{30}$$

To minimize computational errors and achieve higher precision, it becomes necessary to account for variations in the gravitational coupling coefficient *a*, thus requiring the reformulation of Equation (30) as follows:

$$a_{nlf}^2 = \frac{K^2}{2(1+b)^2 n^2}\left(\sqrt{1+\frac{4(1+b)^4 n^4}{K^2}} - 1\right), \; K = \begin{cases} \left[1+\dfrac{a_{nl}^2 g_e g_p}{3(1+b)^2 n}\right] a_{nl}^2 \beta_{nl}, f = 1 \\ \left[1-\dfrac{a_{nl}^2 g_e g_p}{(1+b)^2 n}\right] a_{nl}^2 \beta_{nl}, \; f = 0 \end{cases} \tag{31}$$

The following parameters were adopted for calculations:

Electron *g*-factor: $g_e = 2 \times 1.00115965218076$;

Proton *g*-factor: $g_p = 5.58569469/1836.15266 \approx 1/328.7241358335$;

Electron rest mass: $m_e = 510{,}998.928$ eV;

Proton-to-electron rest mass ratio: $b_0 \approx 1/1836.152669971942$;

Dynamic mass ratio ($n = 1$): $b \approx 1/1836.1038351084 = 0.0005446315077$;

Gravitational coupling coefficient (Lamb shift corrected): $a \approx 1/137.0379202$;

Relativistic correction factor ($n = 1$, $l = 0$): $\beta_{10} = 1.000026597013$;

Using the Planck constant $h = 6.62606957(11) \times 10^3$ J·s and the elementary charge $e = 1.602176565\ (35) \times 10^{-19}$ C, we derive the following conversion relationship:

$$1 \text{ eV} = (e/h) \text{ Hz} \approx 241{,}798.9349604731 \text{ GHz};$$

Substituting these parameters into Equation (31), the calculated gravitational coupling coefficients a for respective quantum states are as follows:

$$a_{nlf} = \begin{cases} n = 1, l = 0, f = 1, a_{101} = 1/137.037927599954025206123 \\ n = 1, l = 0, f = 0, a_{100} = 1/137.037898000399784881604 \end{cases} \tag{32}$$

These represent the gravitational coupling coefficients a_{nlf} between protons and electrons for the two spin configurations. While the difference is minute, it fundamentally revises our previous assumption that the coupling coefficients were identical across quantum states. Substituting these two calculated a-values into Equation (21), we obtain the mass difference for different *f*-state hydrogen atoms at the $n = 1$ principal quantum level:

$$\left.\begin{aligned} E_{101} &\approx -13.5980845804222370525 \text{ eV} \\ E_{100} &\approx -13.5980904547481579742 \text{ eV} \end{aligned}\right\} \Delta E \approx 5.874325920922 \times 10^{-6} \text{ eV} \tag{33}$$

Since 1 eV≈ 241,798.934 960 473 1 GHz, the conversion result is: $\Delta E \approx 1.420405751289589716$ GHz.

The experimentally measured value is 1.4204057517667(10) GHz. This is the famous 21-centimeter hydrogen line in cosmic radiation. This study employs Liu Ziyi's method to calculate the 21 cm hydrogen spectral line frequency, yet obtains results that show remarkable agreement with experimental values. The previous theoretical calculation yielded a precise value of 1.4204034(13) GHz (refer: V.W. Hughes. In ATOMIC PHYSICS 10, edi. by H. Narumi and I. Shimamura. Elsevier Sci. Pub. 1987). The latest CODATA 2023 revision has once again updated the electron-to-proton mass ratio, indicating that our calculations are still not entirely precise. Indeed, achieving such precise theoretical calculations necessarily depends on the accuracy of the Lamb shift measurement. Therefore, these calculations also serve as a means to verify the Lamb shift, while further research on the Lamb shift proves highly beneficial and stimulating.

2.6. How to Incorporate Astrophysics into Quantum Mechanics

According to the period equation for elliptical orbits:

$$m_1\left(\frac{2\pi}{T}\right)r_1 \approx \frac{a}{(1+b)r_1^2} \to T \approx 2\pi\sqrt{\frac{(1+b)m_1 r_1^3}{a}}, a = \frac{Gm_1m_2}{c\hbar} \tag{34}$$

Here, m_1 is the mass of the Earth and m_2 is the mass of the Sun. The mass of the Earth is about 6×10^{24} kg, and the mass of the Sun is about 2×10^{30} kg. The force coefficient a between Earth and the Sun is derived from the law of universal gravitation, expressed as:

$$a = \frac{Gm_1m_2}{c\hbar} \approx \frac{6.67\times10^{-11}\times2\times10^{30}\times6\times10^{24}}{3\times10^{8}\times1.055\times10^{-34}}(\mathrm{SI}) \approx 2.52\times10^{70} \tag{35}$$

The "SI" in the equation indicates that all units are in the International System of Units. According to human measurements and estimates, the average speed of the Earth's orbit around the Sun is 29.8 km/s $\approx 10^{-4}c$. This value can also be used to calculate the gravitational parameter of the Earth-Sun system. Be careful to convert to natural units, $v_1 = 2.98 \times 10^4$ m/s $\approx 10^{-4}$, $c = 1$. This is consistent with the results calculated using quantum mechanical formulas.

$$\left.\begin{array}{l} n = (1+b)\dfrac{m_1v_1r_1}{\hbar} = 2.52\times10^{74}, a = (1+b)nv_1 \\ n\hbar = (1+b)m_1v_1r_1, b \approx 0, v_1 = 10^{-4}, c = 1 \end{array}\right\} a \approx 2.52\times10^{70} \tag{36}$$

Quantization phenomena are the statistical outcomes of a large number of particles (See **Figure 3**).

The smaller the perihelion of an elliptical orbit radius, the larger its aphelion becomes, consequently increasing orbital uncertainty. This demonstrates that the radius of microscopic particles coincides with planetary radii, strictly obeying point-mass mechanics while simultaneously complying with both quantum mechanical and relativistic principles. The perfect unification of relativity and quantum theory represents the correct path forward for the next stage of physics development. According to Equation (36), the principal quantum levels of the nine planets of the Solar System are calculated (see **Table 4**).

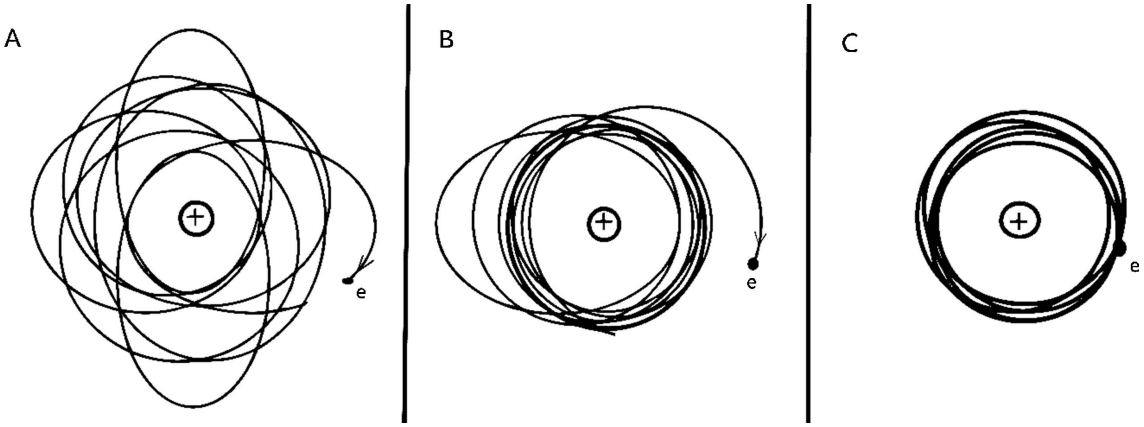

Figure 3. An electron rotates around a proton at a frequency of 6.6×10^{15} cycles per second. The figure depicts only 10 cycles of its trajectory. A. If unaffected by any external influences, an electron captured by a proton would continue orbiting indefinitely along an elliptical trajectory, analogous to a comet's path; B. At the orbit's apogee (farthest point), even a slight momentum perturbation could cause the particle to escape, subsequently being captured by other particles. The proton then recaptures another electron, ultimately retaining only particles conforming to quantized orbits. This selection process typically completes within 10^{-9} seconds; C. The remaining electrons move along quantized orbits, with permitted particle kinetic energy fluctuating within a certain range, conforming to the uncertainty principle. Consequently, energy levels manifest as bands rather than discrete lines. This also explains why comets in the solar system are more prone to disintegration.

Table 4. Principal quantum series n values for the nine planets of the solar system.

Planet	Radius (AU)	Planetary mass (kg)	Quantum number	The n of electron
Mercury	0.39	3.3×10^{23}	$n = 8.9 \times 10^{72}$	$n = 2.43 \times 10^{19}$
Venus	0.72	4.87×10^{24}	$n = 1.75 \times 10^{74}$	$n = 3.24 \times 10^{19}$
Earth	1	5.97×10^{24}	$n = 2.52 \times 10^{74}$	$n = 3.84 \times 10^{19}$
Mars	1.52	6.42×10^{23}	$n = 3.6 \times 10^{72}$	$n = 5.07 \times 10^{19}$
Star cluster	-	-	-	$n = 6.68 \times 10^{19}$
Jupiter	5.2	1.9×10^{27}	$n = 1.84 \times 10^{77}$	$n = 8.71 \times 10^{19}$
Saturn	9.59	5.68×10^{26}	$n = 7.44 \times 10^{76}$	$n = 11.8 \times 10^{19}$
Uranus	19.22	8.68×10^{25}	$n = 1.63 \times 10^{76}$	$n = 16.9 \times 10^{19}$
Neptune	49.2	1.025×10^{26}	$n = 2.18 \times 10^{77}$	$n = 21.2 \times 10^{19}$
Pluto	30.07	1.27×10^{22}	$n = 4.1 \times 10^{72}$	$n = 29.1 \times 10^{19}$

The star cluster mentioned in the table refers to a scattered planetary belt composed of numerous small celestial bodies. From Table 4, the principal quantum number n does not follow an obvious pattern. However, if planetary masses are hypothetically replaced with identical masses, e.g., imagining free electrons occupying the same orbits as planets, the motion of electrons orbiting the Sun would also exhibit quantized orbits. In this scenario, the calculated n-values show a nearly geometric progression pattern. This regularity arises because the quantum number n is extremely large. This observation suggests that during the early formation of the solar system, an explosive event likely generated numerous dust

particles or micro-particles with similar masses. These particles gradually coalesced into planets through quantized orbital aggregation. Calculations indicate that most celestial bodies do not possess quantized orbits with $n = 1$. This is also a consequence of particles aggregating to form larger objects. The Earth's aphelion distance is 1.52×10^{11} m, perihelion distance is 1.471×10^{11} m, with an average orbital speed of 2.98×10^{4} m/s $\approx 10^{-4}c$. Calculate the value of the orbital angular quantum number l for Earth's orbit using the equation:

$$\left.\begin{array}{l} r_A \approx \dfrac{L\hbar}{mv_A}, r_B \approx \dfrac{L\hbar}{mv_A}, v = \dfrac{a}{n}, m = 5.97\times10^{24}\ \text{kg} \\ v_A \approx \dfrac{a}{L}\left(1-\sqrt{1-\dfrac{L^2}{n^2}}\right), v_B \approx \dfrac{a}{L}\left(1+\sqrt{1-\dfrac{L^2}{n^2}}\right) \end{array}\right\} \Delta r \approx \frac{2\hbar\sqrt{n^2-L^2}}{mv} = 5\times10^{9}\ \text{m} \quad (37)$$

We use the Bohr radius substitution method to calculate the results as follows:

$$\left.\begin{array}{l} A:\Delta r = \dfrac{2\hbar\sqrt{n^2-L^2}}{mv} \approx \dfrac{2\hbar\sqrt{n^2-L^2}}{6\times10^{24}\ \text{kg}\times10^{-4}} = 5\times10^{9}\ \text{m} \\ B:a_0 = \dfrac{\hbar}{m_e v_e} \approx \dfrac{\hbar}{9.1\times10^{-31}\ \text{kg}\times(1/137)} = 5.3\times10^{-11}\ \text{m} \end{array}\right\} \frac{A}{B}: n^2 - L^2 \approx 2.04\times10^{145} \quad (38)$$

Here, a_0 is the Bohr radius. The calculations reveal that the values of L and n are nearly identical:

$$\left.\begin{array}{l} n^2 - L^2 = 2.04\times10^{145} \\ n = 2.52\times10^{74} \end{array}\right\} L \approx \sqrt{6.35\times10^{148} - 2.04\times10^{145}} \approx 2.5195\times10^{74} \quad (39)$$

Then, $a = 2.5 \times 10^{70}$, $v = a/n = 10^{-4}$, $n \approx l \approx 2.52 \times 10^{74}$, $b \approx 0$, substituted into Equation (21) to calculate the total rest mass of the Earth and the Sun combined into a two-body particle:

$$M \approx m_{10}\left(1-\frac{v_1^2}{2}\right) + m_{20} \quad (40)$$

Here, m_{10} is the rest mass of the Earth, and m_{20} denotes the rest mass of the Sun. This indicates that after Earth was gravitationally captured by the Sun, it would need to release energy equivalent to its own kinetic energy. This rule is identical to the principle of energy release when an electron is captured by a proton in a hydrogen atom.

2.7. The Magnetic Moment and Radius of an Electron

We have long been perplexed by the formation mechanism of electron magnetic moment. For a moving charge observed perpendicular to its direction of motion, applying the relativistic factor to the electric field and current is equivalent to applying the relativistic factor directly to the charge itself. In multi-charge systems, all orbital charges generate magnetic moments, and the total orbital magnetic moment is the superposition of these individual orbital magnetic moments. Therefore, when observed from the particle's center-of-mass reference frame, the total orbital magnetic moment for a rotating two-body particle system can be expressed as:

$$\mu_l \approx \frac{e_1 v_1 r_1 \beta_1}{2} + \frac{e_2 v_2 r_2 \beta_2}{2} \approx \frac{\left(e_1 + b_0 b e_2\right) L}{2 m_{10} \left(1+b\right)}, b_0 = \frac{m_{10}}{m_{20}}, b = \frac{m_{10} \beta_1}{m_{20} \beta_2} \tag{41}$$

When two magnetic moments approach each other, mutual interference occurs, causing both the particle radii and their magnetic moments to increase, though with differing magnitudes. Precise calculation of these variations remains challenging due to dependencies on multiple factors, including the velocity and directional dynamics of internal charges. Here, we present an approximate computational framework to address this phenomenon. In the magnetic field formed by protons, the radius of the circular motion of each positive charge of neutrons will decrease, while that of each negative charge will increase. Other than that, the speed of the charge's movement will not change. This leads to an increase in the magnetic moment value formed by each negative charge and a decrease in the magnetic moment value formed by each positive charge (see Figure 4).

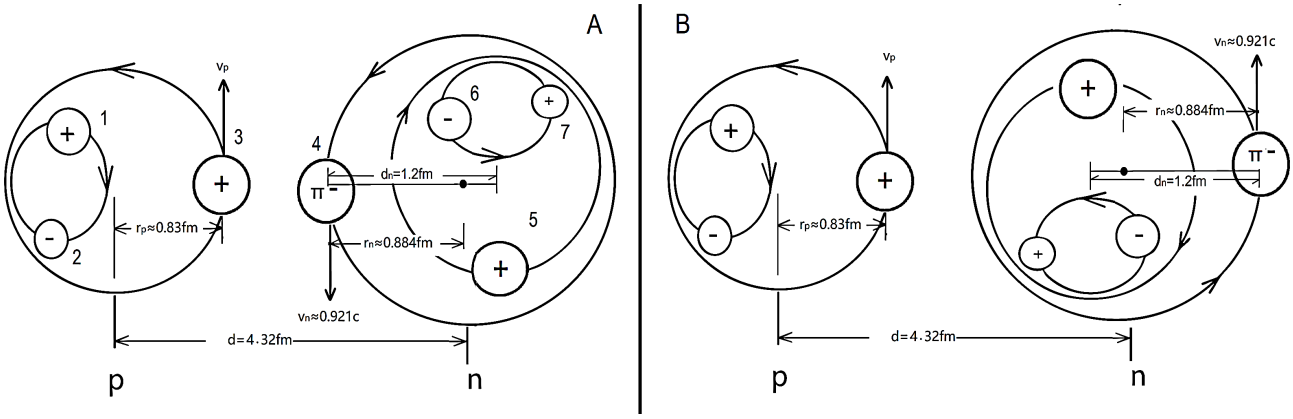

Figure 4. The charge distribution when protons and neutrons combine to form composite particles. The structural derivation of the proton in the figure is detailed in Subsection 2.9. A. The charge distribution inside the deuterium nucleus. B. The possible charge distribution after a certain period of time.

In a deuterium nucleus, the magnetic moment of the proton exerts an electromagnetic force on the π meson within the neutron, causing it to move away from the neutron. This is equivalent to the π meson experiencing a reduced central gravitational force. Considering the relativistic effect, as shown in Figure 4(A), the average force on the valence charge within the neutron is expressed as:

$$\frac{m_\pi v^2}{r_n'} \approx \frac{a_n}{d_n^2} - \frac{1}{\left(d - r_n - r_p\right)^2} \beta_{n+p}, v_{n+p} = \frac{v_n + v_p}{1 + v_n v_p} \tag{42}$$

We provide an estimation method here. According to Equation (14), we estimated the result as:

$$\left.\begin{array}{l} r_n' \approx \dfrac{r_n}{1 - \dfrac{d_n^2}{\left(d - r_n - r_p\right)^2} \dfrac{a_e}{a_n} \beta_{p+n}}, a_n \approx 2.5, d_n = 1.2 \text{ fm} \\ r_n \approx 0.884 \text{ fm}, r_p \approx 0.83 \text{ fm}, d = 4.32 \text{ fm}, v_{n+p} \approx 0.997 \end{array}\right\} r_n' \approx 1.0087 r_n \tag{43}$$

Here, r' is the changed neutron radius, d_n = 1.2fm is the neutron diameter, as shown in **Figure 4(A)**. The increase in the neutron radius results in a change in the neutron magnetic moment of approximately:

$$\Delta\mu_n = v_n\left(r_n' - r_n\right)\frac{e_1 + b_0 be_2}{2\sqrt{1-v_n^2}} \approx 0.0087\times 1.913\mu_N \approx -0.0166\mu_N \tag{44}$$

In Equation (44), we only considered the change of the magnetic moment of motion of the charge 4 within the neutron. When considering the cumulative variations from all internal charged constituents, the net predicted variation in the neutron's magnetic moment amounts to approximately $-0.035\mu_N$. Similarly, within the neutron's magnetic field, the proton's magnetic moment also undergoes modification. While current theoretical frameworks cannot precisely calculate this perturbation, empirical estimates suggest a shift of about $+0.012\mu_n$. The total magnetic moment of the deuteron spin is:

$$\left.\begin{array}{l}\mu_D \approx \dfrac{\left(e_1 + b_0 be_2\right)m_s\hbar}{2\left(1+b\right)m_p} + \mu_p - \mu_n - 0.035\mu_N + 0.012\mu_N \\ n=1, m_s = 0, e_1 = 1, e_2 = 0, \mu_p \approx 2.7928\mu_N, \mu_n \approx 1.913\mu_N\end{array}\right\} \mu_D \approx 0.857\mu_N \tag{45}$$

The orbital magnetic moment projection along the spin axis is quantized as m_s. Some scholars believe that the anomalous magnetic moment of the deuteron is due to part of the deuteron being in the 3D state [14] [15]. However, our explanation is more credible because the same method can account for the other particles magnetic moment. Moreover, all composite particles exhibit a universal magnetic moment behavior: the net magnetic moment never exactly equals the strict vector sum of constituent particles' intrinsic moments, but rather demonstrates subtle deviations. For instance, in the npn particle system (tritium nucleus, ^{3}H), the observed variation measures approximately +0.18616 μ_N.

$$\left.\begin{array}{l}\mu_{npn} \approx \dfrac{\left(e_1 + b_0 be_2\right)m_s\hbar}{2\left(1+b\right)m_n} + \mu_n - \mu_n + \mu_p + \Delta\mu_p \\ n=1, m_s = 0, \mu_p \approx 2.7928\mu_N, \Delta\mu_p \approx 0.18616\mu_N\end{array}\right\} \mu_{npn} \approx 2.97896\mu_N \tag{46}$$

For the pnp particle system (^{3}He nucleus), the magnetic moment variation measures approximately −0.21575 nuclear magnetons (μ_n). The magnetic moment of the helium-3 nucleus is given by:

$$\left.\begin{array}{l}\mu_{pnp} \approx \dfrac{\left(e_1 + b_0 be_2\right)m_s\hbar}{2\left(1+b\right)m_p} + \mu_n + \mu_p - \mu_p + \Delta\mu_n \\ n=1, m_s = 0, \mu_n \approx -1.913\mu_N, \Delta\mu_n \approx -0.21475\mu_N\end{array}\right\} \mu_{pnp} \approx -2.12775\mu_N \tag{47}$$

Professor Samuel C.C. Ting conducted experiments exploring the electron's structure, revealing no structural features at 10^{-18} m. In 1987, Hans Georg Dehmelt and colleagues used electromagnetic trapping experiments to determine that the electron's radius is less than 10^{-22} m (Refer to Dehmelt's 1989 Nobel Prize lecture). For decades, people could not understand why the electron's radius was so small, and many assumed that it was a point particle, which led to an inability to explain

how the electron's spin and magnetic moment were produced.

Based on our derived radius and magnetic moment formulas, the internal charged constituents of an electron can only be very light charged particles, with muons (μ) being the sole candidates satisfying these constraints. Further theoretical investigation reveals that when a muon (mass ≈ 106 MeV) combines with a Z boson (mass ≈ 91 GeV) under radius collapse to 2.53×10^{-21} m in the $n = 413$ excited state, the resulting composite system precisely reproduces the electron's measured mass and magnetic moment. To identify which particles, when combined with the Z boson, yield a radius and magnetic moment consistent with experimental values, we present the calculated results for various candidate particles in Table 5.

Table 5. Possible radius values when particles of different masses are coupled with the Z^0 boson to produce electrons.

Original mass(eV)	Orbital speed(c)	Theoretical radius(m)	Possible hierarchy	Resultant mass(eV)	Magnetic moment(μ_B)	Relativistic gain rate
3.6M + 91G	0.(19N)75	8.56×10^{-23}	n = 14	0.511M	1.00116	4.47×10^{9}
68.5M + 91G	0.(17N)096	8.2×10^{-22}	n = 134	0.511M	1.00116	2.35×10^{8}
96M + 91G	0.16N822	2.3×10^{-21}	n = 375	0.511M	1.00116	1.68×10^{8}
106M + 91G	0.(16N)785	2.53×10^{-21}	n = 413	0.511M	1.00116	1.52×10^{8}
139M + 91G	0.(16N)628	3.3×10^{-21}	n = 544	0.511M	1.00116	1.16×10^{8}
494M + 91G	0.(15N)53	1.1×10^{-20}	n = 1,933	0.511M	1.00116	3.26×10^{7}
1,320M + 91G	0.(14N)664	3.1×10^{-20}	n = 5,166	0.511M	1.00116	1.22×10^{7}

The underlined words are basically consistent with the experiment. 1G = 1000 M.

Assuming the electron is synthesized from μ- and the Z^0 boson, the electron radius is:

$$\left.\begin{array}{l} r_e \approx \dfrac{n\sqrt{1-v^2}\hbar}{(1+b)m_\mu v}, n = 413, b = 0.(10N)824 \\ v = 0.(16N)785c, m_\mu \approx 105.65837 \text{ MeV}, c = 1 \end{array}\right\} r_e \approx -2.53\times10^{-21} \text{ m} \quad (48)$$

The magnetic moment of the electron is:

$$\left.\begin{array}{l} \mu_e \approx \dfrac{(e_1 + b_0 b e_2)m_s\hbar}{2(1+b)m_\mu} + \mu_\mu + \mu_0, \mu_0 \approx 0, e_1 = -1 \\ m_s = 412, e_2 = 0, b \approx 1, \mu_\mu \approx -0.004842371\mu_B \end{array}\right\} \mu_e \approx -1.001159652\mu_B \quad (49)$$

The quantum mechanical representation formula of the electronic magnetic moment is:

$$s = \frac{1}{2}, g_s = 2\times1.00115962 \rightarrow \mu_e = -sg_s\mu_B \approx -1.00115962\mu_B \quad (50)$$

The 2010 Committee on Data for Science and Technology (CDST) provided

that:

The average mass of the muon as 105.6583715(35); The magnetic moment of the muon as $\mu_\mu = 8.89059697(22)\mu_N \approx 0.004842371\mu_B$; The magnetic moment of the electron as $\mu_e = 1.00115965218618076(27)\mu_B$.

We propose that while a free electron exhibits a characteristic radius of 10^{-21} m, its spatial extension undergoes significant contraction when subjected to strong negative magnetic confinement. This phenomenon arises from the circular motion of the electron's negative charge within the opposing magnetic field, resulting in measurable radius reduction—consistent with Dehmelt's experimental observations where confined electrons demonstrated radii below 10^{-22} m [16] [17].

2.8. The Strong Interaction between a Proton and a Neutron

Because such reactions have been observed experimentally [18]:

$$\begin{aligned} &A: \gamma + p^+ \to n + \pi^+ \to p^+ + \pi^0 \\ &B: \pi^+ + p^+ \to \pi^+ + \pi^+ + n \end{aligned} \tag{51}$$

The reaction process described by Equation (51A) is as follows: When a photon collides with a proton, π and π particles are produced. Subsequently, the π particle combines with the proton to form a neutron. Next, the positively charged π strips the negatively charged π from the neutron, synthesizing a neutral π particle. The neutron, now stripped of mesons, reverts to a proton. Similarly, Equation (51B) illustrates that when a π collides with a proton, it generates π and π particles. The π particle then combines with the proton to form a neutron. Our research has demonstrated that as a particle's quantum state approaches annihilation, only a single state exists at the sublevel where $l = n - 1$, then, Equation (21) simplifies to:

$$M = \frac{(1+b)m_{10}}{\sqrt{1-v_1^2}}\left(\frac{1}{b} - v_1^2\right), b^2 = \frac{1}{B^2 - v_1^2\left(B^2 - 1\right)}, B = \frac{1}{b_0} = \frac{m_{20}}{m_{10}} \tag{52}$$

The following table shows the quantum parameters for the formation of neutrons by various mesons and protons to compare which scenario is most likely. **Table 6** shows the results calculated using Equation (52).

Table 6. Compare the possible structures of neutrons.

particle mass (MeV)	Mass ratio	Orbital speed (c)	Ground state radius (fm)	Radius (fm)	Resultant mass (MeV)	Magnetic moment (μ_N)	Quantum level
π139.6 + p938.3	0.3603	0.921	0.442	0.884	939.57	−1.913	$n = 2$
K493.7 + p938.3	0.778	0.866	0.131	0.912	939.57	−1.061	$n = 7$
ρ775 + p938.3	0.945	0.862	0.077	0.848	939.68	+1.661	$n = 11$

Table 6 presents the resulting radii and orbital velocities when composite particles formed from different initial particles reach a mass equivalent to that of a neutron. Here p938.3 represents a proton with a mass of 938.3. The experimentally measured neutron radius ranges from 0.8 to 0.9 fm. We incorporated this

factor when determining the value of n. The underlined data are in agreement with the experiment. From **Table 6**, we can get the following results: A neutron is synthesized from a π-meson and a proton, the radius of a neutron is calculated to be 0.884 fm, with a spin rate of $v_n = 0.921c$, mass ratio $b = 0.36$, existing in the quantum state of $n = 2$, so $m_s = 1$. We present the equation for calculating the magnetic moment of the neutron:

$$\left.\begin{array}{l}\mu_n = \dfrac{(e_1 + b_0 b e_2) m_s \hbar}{2(1+b) m_\pi} + \mu_p + \mu_\pi, \mu_p \approx 2.7928\mu_N, m_s = 1 \\ e_1 = -1, e_2 = 1, b \approx 0.36, b_0 = \dfrac{m_\pi}{m_p} \approx 0.148752, \mu_\pi \approx -0.0274\mu_N\end{array}\right\} \mu_n \approx -1.913\mu_N \quad (53)$$

All magnetic moments discussed herein are defined by their spin-axis projections. The orbital magnetic moment projection along the spin axis is quantized as m_s. Since a neutron transforms into a proton by losing a π meson, it is said that a π meson is exchanged when a neutron and a proton transition between each other. This aligns closely with Hideki Yukawa's theory.

When a proton and a neutron form a deuteron, the binding energy is approximately 2.224 MeV. Therefore, the calculated orbital velocity of the proton is about $0.0489c$. According to Equation (36), the gravitational coefficient between the proton and the neutron is: $a = (1 + b)nv_1 \approx 1/10.22$. In Section 2.9, we provide a detailed method for calculating this gravitational coefficient and demonstrate that the gravitational force between protons and neutrons still arises from the rotational motion of charges (See Equation (56)). From this, it can be seen that the exchange of gluons between protons and neutrons is not the essence of the strong interaction. Rather, the rotation of particles and their charge distribution constitute the fundamental cause underlying the formation of the strong interaction.

2.9. Explore the Structure of Protons

The calculation of three-body particle systems is complex, but still strictly abide by the quantum rules. For instance, when an atomic nucleus captures two electrons, forming a helium-like ion, the binding energy of the second captured electron involves three-body computations. Our proposed formula for this is:

$$\left.\begin{array}{l}W_1 = E_0\left[Z(Z-0)-0\right] \\ W_2 = E_0\left[Z(Z-1)-\sigma\right] \\ \sigma \approx \sum_{i=1}^{i=k} \dfrac{i^2-1}{2^{2n} i^{2n}}, n = 1 \\ E_0 \approx 13.6 \text{ eV}, k = Z\end{array}\right\} \left\{\begin{array}{l}Z = 2, W_2 = E_0\left(2 - \dfrac{3}{4^2}\right) \approx 24.65 \text{ eV}\,(24.6 \text{ eV}) \\ Z = 3, W_2 = E_0\left(6 - \dfrac{3}{4^2} - \dfrac{8}{36}\right) \approx 76 \text{ eV}\,(75.5 \text{ eV}) \\ Z = 6, W_2 = E_0\left(30 - \dfrac{3}{4^2} - \cdots - \dfrac{35}{12^2}\right) \approx 392.7 \text{ eV}\,(392.2 \text{ eV})\end{array}\right. \quad (54)$$

The data in parentheses are experimental values, σ is the potential energy adjustment term of the repulsive force between electrons. Further research demonstrates that atomic nuclei capturing additional electrons follow the same rule. For example, when a carbon nucleus (+6 charge) captures its 3rd electron, the binding

energy is E_3 = 64.5 eV. For the 4th, 5th, and 6th electrons, the binding energies are:

$$\left.\begin{array}{l}\sigma \approx \sum_{i=1}^{i=k} \frac{i^2-1}{2^{2n} i^{2n}} \\ E_3 \approx 64.5 \text{ eV} \\ E_0 = \frac{E_3}{4^2}, n=2 \\ Z=4, k=1,2,3,4\end{array}\right\} \begin{cases} W_3 = E_0\left[Z(Z-0)-0\right] = E_0(16-0) = 16E_0 = 64.5 \text{ eV}(64.5 \text{ eV}) \\ W_4 = E_0\left[Z(Z-1)-\sigma\right] = E_0\left(12-\frac{3}{4^4}\right) \approx 48.33 \text{ eV}(48.6 \text{ eV}) \\ W_5 = E_0\left[(Z-1)(Z-2)-\sigma\right] = E_0\left(6-\frac{3}{4^4}-\frac{8}{6^4}\right) \approx 24.14 \text{ eV}(24.38 \text{ eV}) \\ W_6 = E_0\left[(Z-1)(Z-3)-\sigma\right] = E_0\left(3-\frac{3}{4^4}-\cdots-\frac{15}{8^4}\right) = 12 \text{ eV}(11.26 \text{ eV}) \end{cases} \quad (55)$$

Composite particles often exhibit hybridization and superposition between quantized vibrational and rotational energy levels. However, the rotational energy spectrum vanishes when the central particle's charge distribution is spherically symmetric or when the particle radius becomes sufficiently small. In any case, when internal particles possess sufficiently small radii, they can be treated as point-like particles. This approximation allows the proton to be modeled as a two-body system, albeit introducing significant theoretical errors. Nevertheless, this approach serves as an effective method for inferring proton structure. Experimental studies have determined the proton radius to be approximately 0.83 fm or 0.87 fm [19], while the proton-neutron binding energy yields the strong interaction coefficient a = 1/10.22. Referring to **Figure 4(A)**, we derive the following equation by neglecting less significant terms and introducing an error coefficient σ:

$$\left.\begin{array}{l}\sigma a_e \beta_{n+p} \frac{1+\left(r_p+r_n\right)^2/d^2}{\left[1-\left(r_p+r_n\right)^2/d^2\right]^2} - d^2 F_0 \approx \frac{1}{10.22} \\ v_n \approx 0.921, d \approx 4.32 \text{ fm}, r_n \approx 0.884 \text{ fm} \\ F_0 \approx \frac{\sigma a_e}{d^2}\beta_{n+p} - F_{3*(6+7)}, v_{n+p} = \frac{v_p+v_n}{1+v_p v_n}\end{array}\right\} \begin{cases} r_p = 0.81 \text{ fm} \begin{cases} \sigma = 1/\pi, v_p \approx 0.9974 \\ \sigma = 1, v_p \approx 0.975 \end{cases} \\ r_p = 0.831 \text{ fm} \begin{cases} \sigma = 1/\pi, v_p \approx 0.9972 \\ \sigma = 1, v_p \approx 0.973 \end{cases} \\ r_p = 0.87 \text{ fm} \begin{cases} \sigma = 1/\pi, v_p \approx 0.9971; \\ \sigma = 1, v_p \approx 0.97 \end{cases} \end{cases} \quad (56)$$

Based on the experimental observation of a resonance quantum state with mass number 1019.5 and total spin S = 1, which is hypothesized to be protonium (a bound state of a proton and an antiproton), we proceed to estimate the internal spin velocity of the constituent particles. Following the methodology applied to the deuteron system, we adapt Equation (17) to this scenario:

$$\left\langle a_{p\bar{p}} \right\rangle_{S=1} \approx \sigma a_e \frac{1+4r_p^2/d^2}{\left(1-4r_p^2/d^2\right)^2} \beta_{2p} = n(1+b)v_1, v_{2p} = \frac{2v_p}{1+v_p^2} \quad (57)$$

According to Equation (21), when the mass of protonium is 1019.5, the orbital velocity of the proton is 0.84c. Assuming it is in the n = 12 state, the orbital radius is 0.819 fm, which implies that even if the proton has no spin, the generated strong interaction is sufficient to cause annihilation. Assuming it is in the n = 13 state, the orbital radius is 0.887 fm. Substituting n = 13 into Equation (57), we obtain:

$$\left.\begin{array}{l}\sigma a_e \dfrac{1+4r_p^2/d^2}{\left(1-4r_p^2/d^2\right)^2}\beta_{2p} \approx 21.84 \\ v_p = \dfrac{1}{v_{2p}} - \sqrt{\dfrac{1}{v_{2p}^2}-1}, d = 1.774 \text{ fm}\end{array}\right\} \begin{cases} r_p = 0.815 \text{ fm} \begin{cases} \sigma = 1/\pi, v_p \approx 0.991; \\ \sigma = 1, v_p \approx 0.943 \end{cases} \\ r_p = 0.831 \text{ fm} \begin{cases} \sigma = 1/\pi, v_p \approx 0.986; \\ \sigma = 1, v_p \approx 0.959 \end{cases} \\ r_p = 0.87 \text{ fm} \begin{cases} \sigma = 1/\pi, v_p \approx 0.864; \\ \sigma = 1, v_p \approx 0.611 \end{cases} \end{cases} \quad (58)$$

Experimental detection has revealed the existence of a protonium state with a mass of 1864 and a total spin $S = 0$. The possible rotational modes of the particle are as shown in Figure 5. Based on this, we obtain Equation (57):

$$\sigma a_e \beta_{2p} \approx 0.23n \begin{cases} n = 1, \sigma = 1/\pi, v_p \approx 0.99; \sigma = 1, v_p \approx 0.968 \\ n = 2, \sigma = 1/\pi, v_p \approx 0.995; \sigma = 1, v_p \approx 0.984 \end{cases} \quad (59)$$

Accounting for error factors, we conclude that the proton's spin rate is approximately 0.91 - 0.99, and its radius is about 0.83 - 0.86 fm. With knowledge of the proton's spin rate and radius, the structure of the proton can be roughly estimated by Equation (14) and Equation (52). Table 7 shows several possible results we calculated.

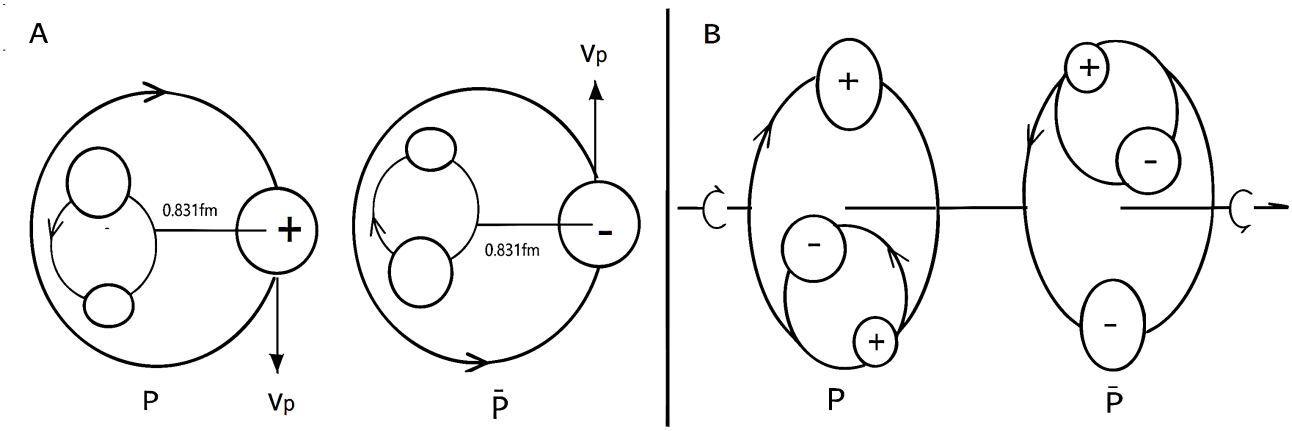

Figure 5. The state of protonium when the total spin is $S = 0$. A. Proton and antiproton with antiparallel spins. B. Proton and antiproton with coaxial counter-rotating spins.

When assuming the proton is composed of a ρ (775) meson and a Σ (1193) baryon, the proton must occupy the $n = 15$ quantum state, otherwise, its orbital radius would deviate from the experimental range of 8.1 - 8.7 fm. The resulting magnetic moment of the proton is:

$$\left.\begin{array}{l}\mu_p \approx \dfrac{m_s \hbar}{2(1+b)m_\rho}\left(e_1 + b_0 b e_2\right) + \mu_\rho + \mu_\Sigma, n = 15, m_s = 14 \\ b = 0.912, e_1 = 1, e_2 = 0, m_\rho \approx 775, \mu_\rho + \mu_\Sigma \approx -6.06\mu_N\end{array}\right\} \mu_n \approx 2.7928\mu_N \quad (60)$$

Of course, this is only a reasonable conjecture. If experimental measurements reveal that the magnetic moment of the Σ (1193) particle is approximately $-6.06\mu_N$, it would provide clear confirmation that the proton indeed has such a

structure. However, until experimental confirmation is obtained, we present this primarily as a reference for readers. The internal structure of particles manifests through their magnetic moments. Precise measurement of particle magnetic moments will therefore serve as an effective method for studying particle internal structures.

Table 7. Spin rates and radius values for certain mesons and baryons when their combined mass is close to that of a proton.

Original Mass (MeV)	Dynamic mass ratio	Orbital speed (c)	Relativistic increment	Theoretical radius (fm)	Possible hierarchy	Resultant mass (MeV)	Central magnetic moment (μ_N)
139 + 1116	0.587	0.9848	5.792	0.81	$n = 5$	938.1	−14.2
139 + 1193	0.6446	0.9902	7.16	0.853	$n = 7$	937.8	−21.9
494 + 1116	0.7958	0.9266	2.659	0.815	$n = 9$	938.5	−5.66
494 + 1193	0.8071	0.943	3.005	0.862	$n = 11$	938.3	−7.7
494 + 1232	0.8125	0.9494	3.184	0.81	$n = 11$	939.2	−7.7
494 + 1315	0.826	0.961	3.616	0.85	$n = 14$	938.3	−10.7
775 + 1193	0.912	0.9237	2.62	0.831	$n = 15$	938.3	−6.06
775 + 1232	0.9109	0.9304	2.728	0.844	$n = 16$	938.1	−6.70
775 + 1315	0.9085	0.942	2.98	0.859	$n = 17$	938.3	−7.33

The underlined data represents the more probable scenario.

3. Results and Conclusions

3.1. The Strong Interaction between a Quark and an Antiquark

The partial data of the J/ψ particle discovered in the experiment are as follows: 2980; 3097; 3415; 3510; 3556; 3594; 3686; 3770; 3823; 3872; 3885; 3900; 3930; 4009; 4022; 4030; 4040; 4160; 4260; 4360; 4415; 4421; 4456; 4664. Some data of ϒ particle that have been experimentally discovered are as follows: 9460; 9859; 9893; 9912; 10,023; 10,233; 10,255; 10,269; 10,355; 10,573; 10,650 (PDG2023) [20]-[22].

First of all, with the mass of the particle, we can calculate the gravitational coefficient inside the particle. Second, based on the theory of relativity, we have established an equation for calculating the gravitational coefficient between quarks. Based on the experimental data, we calculated the gravitational coefficients for each quantum state by Equation (21) and placed them in the "Exp. a" column of Table 8. The gravitational coefficients calculated using Equation (14) are listed in the "Th a" column of Table 8 [11]. If Liu Yun's hypothesis is correct, the gravitational coefficients derived from Equations (21) and (14) will be identical.

From Table 8, it can be observed that the strong interaction between quarks is the total superposition of the relativistic effects of the internal charges of the quarks.

Table 8. Comparison of the coupling coefficient of quark potential strength interaction calculated theoretically with the experimentally measured values.

J/ψ particle					ϒ particle				
Quantum level	*r* (fm)	Exp. *a*	Th. *a*	*M* (MeV)	Quantum level	*r* (fm)	Exp. *a*	Th. *a*	*M* (MeV)
n = 4	0	0	0	0	n = 6	0	0	0	0
n = 5	0.1796	7.310	7.329	3097	n = 7	0.183	7.478	7.476	9460
n = 6	0.347	6.749	6.677	3770	n = 8	0.279	6.975	6.916	10,023
n = 7	0.519	6.611	6.559	4030	n = 9	0.374	6.710	6.718	10,355
n = 8	0.701	6.572	6.518	4160	n = 10	0.497	6.420	6.613	10,573
n = 9	0.934	6.460	6.495	4260	n = 11	0.592	6.575	6.574	10,650

3.2. The Essence of Weak Interaction

The weak interaction was initially proposed to explain beta decay, the process of conversion between protons and neutrons. Experimental observations indicate that the weak interaction is always accompanied by the emission or absorption of neutrinos and invariably results in parity violation.

Between atoms, the mutual interpenetration of orbitals can form covalent bonds, leading to increased stability in multi-particle systems. Research indicates that similar orbital overlap phenomena also exist among microscopic particles. Experiments have detected the "proximity freedom" effect within the strong interaction. As illustrated in Figure 6, this effect only occurs when particle radii interpenetrate, demonstrating that radius overlap between microscopic particles happens frequently.

When the orbits intersect, the internal charge motion of the particles becomes

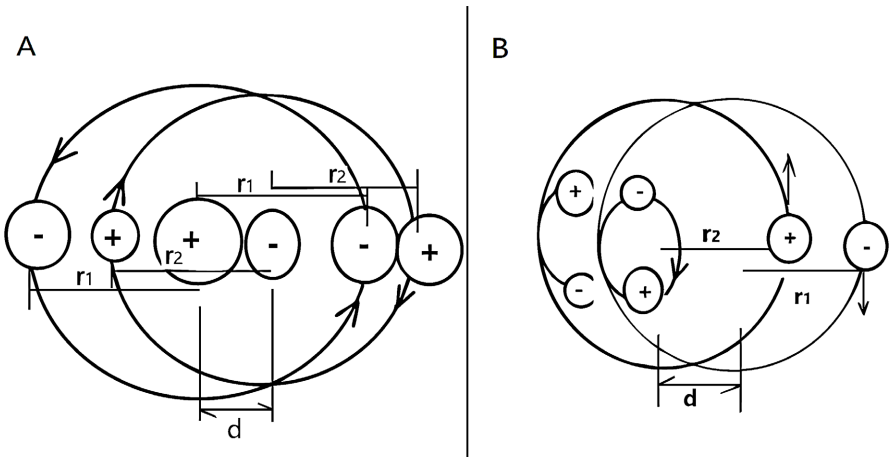

Figure 6. Simplified diagram of the internal charge distribution when the radii of particles with opposite charges interpenetrate and overlap each other. A. The internal charge distribution of particles when the central mass is large. B. Internal charge distribution when approximated as a two-body particle system.

more complex. Figure 6 shows a simplified charge distribution diagram. Assuming the particle radii are not identical and they rotate at extremely high speeds, the gravitational coefficient formula between the particles, as illustrated in Figure 6(B), is:

$$a \approx \frac{1+\Delta^2}{\left(1-\Delta^2\right)^2}\beta_{1+2}, \Delta = \frac{r_1 - r_2}{d} \tag{61}$$

This indicates that a peak in the gravitational coefficient occurs when $d \approx \Delta r$. When $\Delta r = 0$, the two particles behave as particle-antiparticle pairs, and at $d = 0$, the gravitational coefficient reaches its maximum, leading to complete annihilation—a result fully consistent with experimental observations. Only such a structure can explain why the neutrino's magnetic moment is so exceedingly small [23].

The essence of weak interaction lies in either the reaction process, where π mesons and three types of charged leptons produce neutrinos, or the decay process, where neutrinos disintegrate into charged leptons.

The neutron contains one more π meson than the proton. When a free positron approaches a neutron, there is a certain probability that it will intersect and combine with a π meson inside the neutron, forming a very light neutral particle—the electron neutrino. Some studies suggest that neutrinos lack parity. Therefore, to ensure parity conservation in this reaction, participating gluons (including photons) must be included in the process. The final outcome is equivalent to the neutrino possessing well-defined parity. The reaction equation is as follows:

$$\begin{aligned}
&A: e^-(+) + \pi^+(-) = \nu_e(+) + k\gamma(-) + Q, k = 1,3,\cdots \\
&B: e^+(-) + \pi^-(-) = \overline{\nu}_e(-) + k\gamma(-) + Q, k = 1,3,\cdots \\
&C: \mu^-(+) + \pi^+(-) = \nu_\mu(+) + k\gamma(-) + Q, k = 1,3,\cdots \\
&D: \tau^-(+) + \pi^+(-) = \nu_\tau(+) + k\gamma(-) + Q, k = 1,3,\cdots
\end{aligned} \tag{62}$$

In the equation, we postulate that the electron neutrino has positive parity, γ represents a possible type of gluon (such as a photon) that may be generated, and k denotes the number of generated particles. Q stands for the heat produced in the reaction: $Q > 0$ for reactions where rest mass decreases, $Q < 0$ for reactions where rest mass increases. The signs (±) in parentheses indicate the parity of the particles. Taking the electron neutrino as an example, since both parity and energy are conserved in the reaction equations, we use the "=" sign to denote the balance. By summing ($A + B + C$) and simplifying, we obtain the following equation:

$$\left.\begin{aligned}
&A: e^+(-) + \pi^-(-) = \overline{\nu}_e(-) + k\gamma(-) + Q \\
&B: \mu^-(+) + \pi^+(-) = \nu_\mu(+) + k\gamma(-) + Q \\
&C: k\gamma(-) = e^+(-) + e^-(+) + Q
\end{aligned}\right\} A + B + C \rightarrow$$
$$D: \mu^-(+) = e^-(+) + \overline{\nu}_e(-) + \nu_\mu(+) + k\gamma(-) + Q, k = 1,3,\cdots \tag{63}$$

The same particles on both sides of the equal sign indicate that they are consumed immediately after being produced. When particles combine, their mass de-

creases as their radius shrinks. Thus, when a muon combines with a π meson and the mass reduces to 0.17 MeV (the experimentally observed mass of the muon neutrino), the radius should be approximately 2×10^{-18} m—consistent with the conventionally accepted range of the weak interaction. Summing the following equations yields:

$$\left.\begin{array}{l} k\gamma(-) = e^{-}(+) + e^{+}(-) + Q, k = 1,3... \\ k\gamma(-) + n(+) = p^{+}(+) + \pi^{-}(-) + Q, k = 1,3... \\ \pi^{-}(-) + e^{+}(-) = \overline{\nu}_e(-) + k\gamma(-) + Q, k = 1,3... \end{array}\right\} \rightarrow$$
$$A: n(+) = p^{+}(+) + \overline{\nu}_e(-) + e^{-}(+) + k\gamma(-) + Q, k = 1,3,\cdots \quad (64)$$
$$Q = m_n - m_p - m_{ve} - m_e - m_\gamma$$

This is a composite reaction formed by the superposition of multiple processes. When the negative pion (π^-) inside the neutron has a certain probability of approaching the proton in an elliptical orbit, it converts its potential energy into a photon pair. One of these photons then decays into an electron-positron pair. Subsequently, the positron interacts with the π^- meson, producing a neutrino, while the neutron—now having lost the π^- meson—transforms into a proton. Since the annihilation of half-spin particles and antiparticles produces an odd number of photons, when moving the half-spin particle in the above equation to the other side of the equality sign, it must be replaced by its corresponding antiparticle while simultaneously adding a photon, thus, parity conservation is maintained [18].

$$\left.\begin{array}{l} k\gamma(-) + n(+) = p^{+}(+) + \pi^{-}(-) + Q, k = 1,3... \\ \pi^{-}(-) + e^{+}(-) = \overline{\nu_e}(-) + k\gamma(-) + Q, k = 1,3... \end{array}\right\} \rightarrow$$
$$n(+) + e^{+}(-) = p^{+}(+) + \overline{\nu}_e(-) + k\gamma(+) + Q, k = 0,2,4... \quad (65)$$
$$Q = m_n + m_e - m_p - m_{ve} - m_\gamma$$

Theoretically, precise measurement of the Q-value could determine which specific particles participated in the reaction process. The same method can be applied to the following reaction equations:

$$n(+) = p^{+}(+) + \overline{\nu}_e(-) + e^{-}(+) + k\gamma(-) + Q \rightarrow$$
$$\begin{cases} n(+) + \nu_e(+) = p^{+}(+) + e^{-}(+) + k\gamma(+) + Q, k = 0,2,4,\cdots \\ n(+) + \nu_e(+) + e^{+}(-) = p^{+}(+) + k\gamma(-) + Q, k = 1,3,5,\cdots \end{cases} \quad (66)$$

Experimental observations show that a hydrogen nucleus (a single proton) is highly stable, whereas deuterium nuclei (containing a neutron) frequently undergo β^- decay. However, the photons produced in this process do not necessarily leave the atomic system. Some photons may be absorbed by the atom, subsequently altering the angular quantum number of a particular orbital—a phenomenon well-documented in numerous physical experiments and extensively verified. Since only a portion of the photons are absorbed by the atomic system, the resulting electrons exhibit a continuous energy spectrum ranging from zero to maximum kinetic energy. This observation confirms that parity remains con-

served in weak interactions, although the atomic system itself may sometimes display apparent parity non-conservation. Madame Chien-Shiung Wu's experiment with cobalt-60 nuclei emitting electrons precisely demonstrated this reaction.

Furthermore, the parity ambiguity of K mesons arises precisely due to reactions of the following type:

$$\pi^0(-) \to \pi^+(-) + \pi^-(\perp) \qquad (14\%) \tag{67}$$

Experimental observations reveal that such reactions consistently occur with a probability of 14%, and the two resulting π mesons must have mutually perpendicular spin orientations. This configuration ensures parity conservation in the equation, which is why we add a perpendicularity symbol ($\perp$) to one π meson in the formula.

The very existence of these reactions led to the recognition that π mesons must possess negative parity. Given this understanding, the following reaction should come as no surprise:

$$\begin{aligned} A: &\begin{cases} \pi^+(-) + n(+) \to \tau^+(-) + \Lambda(+), \\ \tau^+(-) \to \pi^+(\perp) + \pi^0(-) \to \pi^-(\perp) + \pi^+(\perp) + \pi^+(-) \quad (14\%) \end{cases} \\ B: &\begin{cases} \pi^+(-) + n(+) \to \theta^+(-) + \Lambda(+), \\ \theta^+(-) \to \pi^+(\perp) + \pi^0(-) \to \pi^+(\perp) + \pi^0(-) \qquad (86\%) \end{cases} \end{aligned} \tag{68}$$

Later, it was discovered that these so-called τ and θ particles were in fact the same K meson. The inability to reconcile their parity conservation led to what became known as the $\tau - \theta$ puzzle. When the decay produced three mesons, the mutual perpendicularity relationship became less obvious, which initially caused confusion. Crucially, these reactions did not involve neutrino exchange and were therefore not weak interaction processes—they were purely strong interaction reactions. As such, parity conservation was absolutely required in these decays.

3.3. Explorations on the Unification of Gravitational and Electromagnetic Forces

Based on our previous arguments, both the strong and weak interactions can be unified within the framework of electromagnetic interaction. However, can gravitational force between masses also be unified into electromagnetic interaction?

Initially, our research group approached this question with a relatively simplistic assumption: we hypothesized that gravitational force between masses might also arise from a superposition of electromagnetic effects. We have gathered some evidence supporting this idea. For instance, although certain particles do not possess a net magnetic moment, they carry oscillating magnetic moments—analogous to alternating currents. When such particles accumulate in large numbers, their collective interaction manifests externally, with the probability of attractive forces (gravitation) consistently exceeding that of repulsive forces (as illustrated in Figure 7).

To demonstrate that gravitational mass originates from electromagnetic inter-

actions between charges, we present the formation mechanism of gravitational attraction in electron-positron bound states (positronium).

As shown in **Figure 7(A)**, when neglecting the influence of internal particle spins and considering only electron spin effects, the instantaneous resultant of electric and magnetic forces between charge pairs 1 + 2 and 3 + 4 can be expressed as (where $S = 1$ denotes spin state, with the negative sign indicating the attractive term):

$$F_{(1+2)*(3+4),S=1} = \frac{a_e}{d^2}\left(q_1q_3\beta_0 - q_1q_4\beta_{2v+2e} - q_2q_3\beta_{2v-2e} + q_2q_4\beta_{2e}\right) \tag{69}$$

Applying the same methodology, the instantaneous resultant force between charge pairs 3 + 4 and 5 + 6 in **Figure 7(A)** is given by ($S = 1$):

$$F_{(5+6)*(3+4),S=1} = \frac{a_e}{d^2}\left(q_5q_3\beta_0 - q_5q_4\beta_{2e} - q_6q_3\beta_{2e+2v} + q_6q_4\beta_0\right) \tag{70}$$

In **Figure 7(B)**, the instantaneous resultant force between charge pairs 1 + 2 and 3 + 4 is given by ($S = 0$):

$$F_{(1+2)*(3+4),S=0} = \frac{a_e}{d^2}\left(q_1q_3\beta_0 - q_1q_4\beta_{2e-2v} - q_2q_3\beta_{2e-2v} + q_2q_4\beta_0\right) \tag{71}$$

In **Figure 7(B)**, the instantaneous resultant force between charge pairs 3 + 4 and 5 + 6 is given by ($S = 0$):

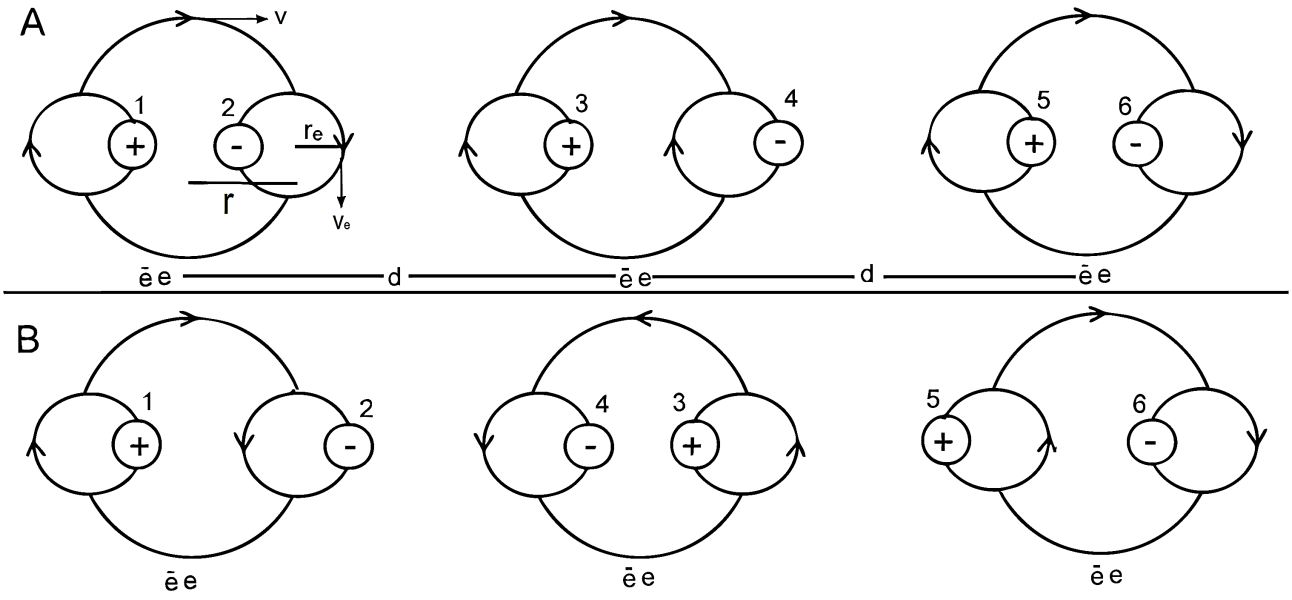

Figure 7. Charge distribution in positronium systems. A. Three positronium with aligned spin orientations. B. Three positronium with anti-aligned spin orientations.

$$F_{(5+6)*(3+4),S=0} = \frac{a_e}{d^2}\left(q_5q_3\beta_{2e} - q_5q_4\beta_{2v} - q_6q_3\beta_{2v} + q_6q_4\beta_0\right) \tag{72}$$

Considering that the electron spin rate is significantly greater than the orbital rate, averaging over the four equations yields a net gravitational attraction. This demonstrates that when numerous particles without magnetic moments aggre-

gate, the probability of gravitational attraction occurring in any given direction is higher than that of repulsion. Furthermore, when accounting for the internal charge motion within particles, and Particle deformation due to the principle of minimum energy state, it becomes evident that magnetic gravitational attraction arises between particles regardless of whether they possess intrinsic magnetic moments. Although this magnetic gravitational force becomes exceedingly weak at long distances, the collective effect of numerous aggregated particles can cumulatively generate sufficient gravitational pull through superposition. This fundamentally explains the origin of mass-induced gravity.

Moreover, if we statistically analyze the force-versus-distance curves of numerous microscopic particles, the averaged trend closely resembles the interaction force profile between molecules (as shown in Figure 8).

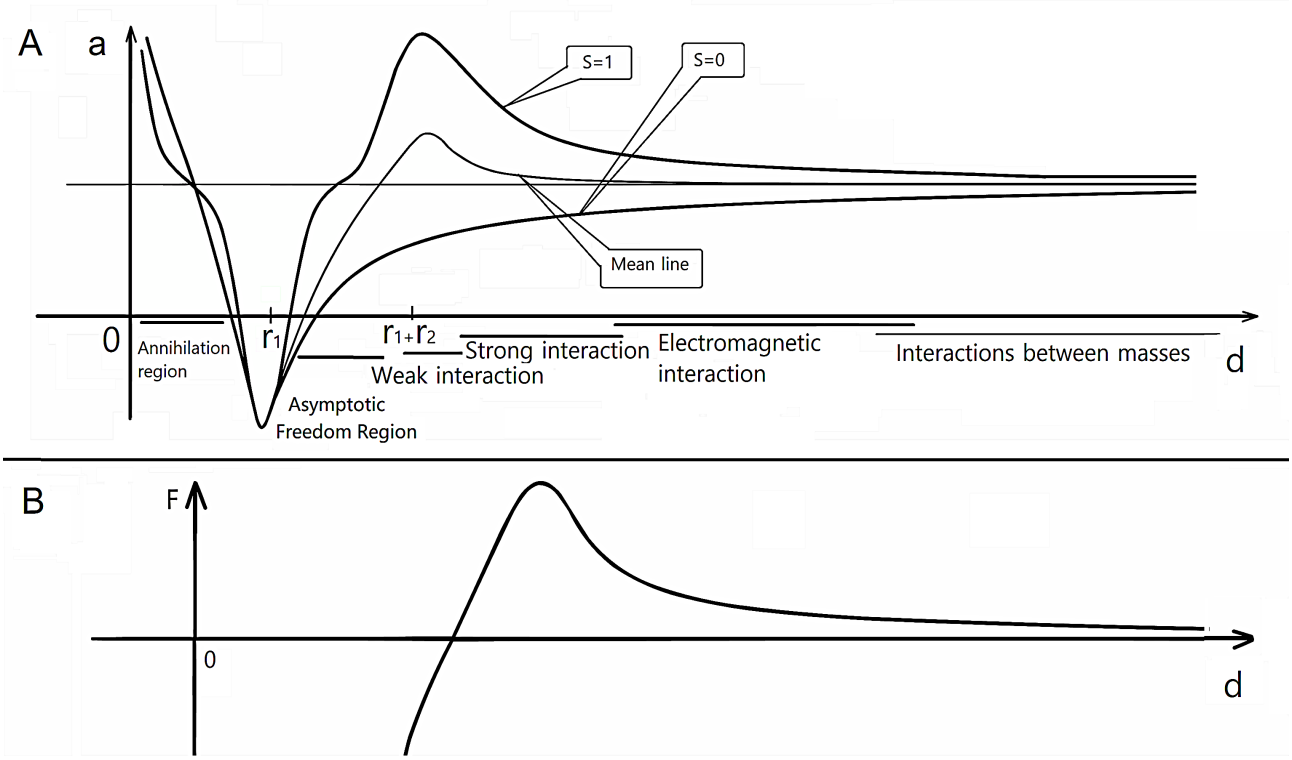

Figure 8. The unity of the four basic interactions. A. The relationship between the interaction coefficient of quarks and distance. B. The relationship between intermolecular forces and distance. This is very similar to the average force line between quarks.

The third evidence we propose is that the gravitational coefficient may not be a constant, but rather a variable parameter. According to the gravitational coefficient equation, the gravitational coefficients between different particles vary. If materials of different compositions are selected for measuring the universal gravitational constant, the results will inevitably differ. This aligns with experimental observations: no two measurements of the gravitational constant have ever been identical, always showing minor discrepancies. Recent experimental reassessments of the gravitational constant by multiple physics research teams have revealed significant discrepancies. For instance, in 2018, the Chinese team led by

Professor Luo Jun at Huazhong University of Science and Technology measured the gravitational constant between tungsten-gold alloy spheres, obtaining a value greater than 6.6742×10^{-11} (SI units) [17] [24], while the average value measured using ordinary spheres was 6.672×10^{-11} (SI units), demonstrating remarkable deviations.

However, after reviewing relevant literature in this field, we have come to recognize that gravitational attraction may involve a more complex mechanism. Einstein once pointed out that gravity does not truly exist as a force; rather, it arises because mass curves the surrounding spacetime, causing objects to follow curved paths instead of straight lines, thus creating the appearance of attraction. In his general theory of relativity, Einstein proposed the Einstein Equivalence Principle (EEP). To fully explain the origin of gravitational attraction, it is necessary to clarify how mass causes the curvature of spacetime while remaining consistent with the EEP.

Around 1960, Leonard Schiff conjectured that this kind of connection was a necessary feature of any self-consistent theory of gravity [25]. More precisely, Schiff's conjecture states that any complete, self-consistent theory of gravity that embodies WEP necessarily embodies EEP. In other words, the validity of WEP alone guarantees the validity of local Lorentz and position invariance, and thereby of EEP.

Given the limited knowledge base of our research group and our incomplete understanding of theoretical physics—particularly in the area of general relativity—we currently lack the capacity to fully resolve this challenging problem. Nevertheless, this question has captured our strong interest. Regardless, the ideas we propose may be regarded as one possible perspective, offering an alternative approach for further exploration. Achieving a true unification of the four fundamental forces will require collaborative efforts from a broader community of physicists.

Acknowledgements

We acknowledge helpful discussions with Professor Xu Zhan, Professor Wang Qing and Professor Zhang Zhi, and we have received substantial assistance from the National Library of China.

Conflicts of Interest

The authors declare no conflicts of interest regarding the publication of this paper.

References

[1] Griffiths, D.J. (2018) Introduction to Elementary Particle. Translated by Q. Wang, Machinery Industry Press, 56-315.

[2] Al-Omari, A. and Noiri, T. (2011) A Unified Theory of Generalized Closed Sets in Weak Structures. *Acta Mathematica Hungarica*, **135**, 174-183. https://doi.org/10.1007/s10474-011-0169-0

[3] Eichten, E., Gottfried, K., Kinoshita, T., Lane, K.D. and Yan, T. (1978) Charmonium: The Model. *Physical Review D*, **17**, 3090-3117. https://doi.org/10.1103/physrevd.17.3090

[4] Eichten, E., Gottfried, K., Kinoshita, T., Lane, K.D. and Yan, T.M. (1980) Charmonium: Comparison with Experiment. *Physical Review D*, **21**, 203-233. https://doi.org/10.1103/physrevd.21.203

[5] Gupta, P. and Mehrotra, I. (2012) Study of Heavy Quarkonium with Energy Dependent Potential. *Journal of Modern Physics*, **3**, 1530-1536. https://doi.org/10.4236/jmp.2012.310189

[6] Kuang, Y. (2006) QCD Multipole Expansion and Hadronic Transitions in Heavy Quarkonium Systems. *Frontiers of Physics in China*, **1**, 19-37. https://doi.org/10.1007/s11467-005-0012-6

[7] Brambilla, N., Pineda, A., Soto, J. and Vairo, A. (2005) Effective-Field Theories for Heavy Quarkonium. *Reviews of Modern Physics*, **77**, 1423-1496. https://doi.org/10.1103/revmodphys.77.1423

[8] Segovia, J., Entem, D.R., Fernández, F. and Ruiz Arriola, E. (2012) Renormalized Quarkonium. *Physical Review D*, **86**, Article ID: 094027. https://doi.org/10.1103/physrevd.86.094027

[9] Ka, X.L. (2001) Advanced Quantum Mechanics. Higher Education Press, 206-207. (In Chinese)

[10] Liu, Y., Liu, Z. and Liu, Z. (2023) New Progress in the Study of Quark Mass Unlock the Secrets of Strong Force. *Advances in Engineering Technology Research*, **4**, 132-139. https://doi.org/10.56028/aetr.4.1.132.2023

[11] Liu, Y., Liu, Z. and Liu, Z.Y. (2024) How Far Is the Ultimate Goal of Physics—Unification of the Strong Force with the Electromagnetic Force. *Modern Physics*, **14**, 196-205. https://doi.org/10.12677/mp.2024.145023

[12] Yang, Y.F. (2020) The Study of Exotic States in Charmonium-Like Quarkonium. Master's Thesis, Nanjing Normal University. (In Chinese) https://doi.org/10.27245/d.cnki.gnjsu.2020.001477

[13] Wang, J.Z. (2022) A Study on the Properties of Charmonium-Like XYZ Particles and Exotic Quarkonium States. Master's Thesis, Lanzhou University. (In Chinese) https://doi.org/10.27204/d.cnki.glzhu.2022.002754

[14] Xu, K.Z., Chen, X.J. and Chen, H.F. (2015) Modern Physics. Science and Technology Press, 240-241. (In Chinese)

[15] Zhang, Q.R. (1964) Non-Localized Force and Deuteron Magnetic Moment. *Journal of Peking University* (*Natural Science*), **4**, 367-372.

[16] D'Onofrio, M., Xie, Y., Rasmusson, A.J., Wolanski, E., Cui, J. and Richerme, P. (2021) Radial Two-Dimensional Ion Crystals in a Linear Paul Trap. *Physical Review Letters*, **127**, Article ID: 020503. https://doi.org/10.1103/physrevlett.127.020503

[17] Li, Q., Xue, C., Liu, J., Wu, J., Yang, S., Shao, C., *et al.* (2018) Measurements of the Gravitational Constant Using Two Independent Methods. *Nature*, **560**, 582-588. https://doi.org/10.1038/s41586-018-0431-5

[18] Lu, X.T. (2009) Nuclear Physics. Atomic Energy Press, 359-360. (In Chinese)

[19] Cai, L. (2019) How Big a Proton Is. *World Science*, **12**, 7.

[20] Zhao, Y.H., Hai, W.H. and Zhu, Q.Q. (2009) Multi-Order Corrections of Variational-Integral Perturbation for Heavy Quarkonium. *Acta Physica Sinica*, **58**, 734-739. https://doi.org/10.7498/aps.58.734

[21] Mei, H. and Chen, H. (2004) Study on Mass Spectra of Heavy Quarkonium by Relativistic Quark Model. *Nuclear Physics Review*, **4**, 300-305.

[22] Nielsen, M. (2015) Charmonium Charged States. *Nuclear and Particle Physics Proceed-*

ings, **258**, 139-143. https://doi.org/10.1016/j.nuclphysbps.2015.01.030

[23] Masood, S.S. (2015) Magnetic Dipole Moment of Neutrino. *Journal of High Energy Physics, Gravitation and Cosmology*, **1**, 1-13. https://doi.org/10.4236/jhepgc.2015.11001

[24] Hu, Q.G. (2022) Experiment on Measuring the Universal Gravitational Constant between a 2 kg Iron Ball and a 20 t Steel Plate 2 kg. *Journal of Normal University Science*, **42**, 48-55.

[25] Will, C.M. (2014) The Confrontation between General Relativity and Experiment. *Living Reviews in Relativity*, **17**, Article No. 4. https://doi.org/10.12942/lrr-2014-4